ANALYSIS OF WAVEGUIDE DISCONTINUITIES BY MMM

ANALYSIS OF WAVEGUIDE DISCONTINUITIES

BY

MODE MATCHING METHOD

By

KAI JIANG, B.S., M.E.

A Thesis

Submitted to the School of Graduate Studies

in Partial Fulfilment of the Requirements

for the Degree

Master of Applied Science

McMaster University

© Copyright by Kai Jiang, 2006

MASTER OF APPLIED SCIENCE (2006) McMaster University

(Electrical and Computer Engineering) Hamilton, Ontario

TITLE: Analysis of Waveguide Discontinuities by Mode Matching Method

AUTHOR: Kai Jiang, B.S., M.E.

SUPERVISOR: Professor W. P. Huang

NUMBER OF PAGES: viii, 58

Abstract

An effective mode matching method (MMM) is developed for dealing with three-dimensional (3D) dielectric waveguide structures with arbitrary transverse index profiles and scattering interfaces along the longitudinal waveguide axis. With the introduction of a perfectly conducting box coated by a perfectly matched layer (PML) as the lateral boundary, the method circumvents the inherent difficulties associated with the continuous radiation modes of open waveguide structures. The semi and full-vectorial finite difference (FD) methods are employed for mode calculation. The guideline for choice of the PML parameters in the mode matching analysis is discussed via a two-dimensional (2D) waveguide structure with a single step discontinuity. We show results for the 3D waveguide air gap, facet and polarization converter. The effectiveness and efficiency of the method are validated.

Acknowledgements

I would like to thank Dr. W. P. Huang for his support, stimulating suggestions, and encouragement in my research work.

Contents

1 Introduction 1
2 Formulations 6
2.1 Modal Solutions 7
2.1.1 1D Multilayer Waveguide Modes 7
2.1.2 2D Waveguide Modes 11
2.2 Mode Matching Solutions 15
2.3 Multiple Waveguide Discontinuities 19
Appendix A: 1D Mode Calculation and Mode Matching 21
A.1 Argument Principle Method (APM) 21
A.2 Smooth Transition Method 23
A.3 Application 23
Appendix B: Finite Difference (FD) Method for Mode Calculation 26
B.1 FD Scheme 27
B.2 Application 30
3 PML Effects on Mode Matching Solutions 33
4 Application to 3D Waveguide Structures 40
4.1 Assessment of the Semi-Vectorial Method 40
4.2 Application 42
4.2.1 Waveguide Air Gap 42
4.2.2 Waveguide Facet 46
4.2.3 Polarization Converter 47
5 Conclusions 52
Bibliography 54

List of Figures

Fig. 1: Leaky waves in a multilayer waveguide. 2
Fig. 2: A multilayer waveguide structure. 7
Fig. 3: A 2D arbitrary waveguide structure surrounded by a perfectly conducting electric box with the inner PML. 11
Fig. 4: A waveguide discontinuity. 16
Fig. 5: Multiple waveguide discontinuities. 19
Fig. 6: A typical double-layer antireflection coated facet. $n_1 = 3.524$, $n_2 = 3.17$, $n_3 = 1.82$, $n_4 = 1.65$, $d_1 = 0.11\,\mu m$, $d_2 = 3.6\,\mu m$, $d_3 = 0.5\,\mu m$, $h_1 = 0.1816\,\mu m$, and wavelength $\lambda = 1.54\,\mu m$ 24
Fig. 7: Normalized propagation constants for the slab waveguide in a typical double-layer antireflection coated facet (TE). $n_1 = 3.524$, $n_2 = 3.17$, $d_1 = 0.11\,\mu m$, $d_2 = 3.6\,\mu m$, $d_3 = 0.5\,\mu m$, and wavelength $\lambda = 1.54\,\mu m$. 25
Fig. 8: Power reflection coefficient versus the second layer film thickness for a typical double-layer antireflection coated facet (TE). $n_1 = 3.524$, $n_2 = 3.17$, $n_3 = 1.82$, $n_4 = 1.65$, $d_1 = 0.11\,\mu m$, $d_2 = 3.6\,\mu m$, $d_3 = 0.5\,\mu m$, $h_1 = 0.1816\,\mu m$, and wavelength $\lambda = 1.54\,\mu m$ 26
Fig. 9: Positions of the nodes for FD scheme. The node is located at the center of the cell and the medium in each cell is uniform. 29
Fig. 10: A typical 3D leaky waveguide. 30
Fig. 11: Electric field distributions of two symmetric quasi-TE modes for a leaky waveguide. 32
Fig. 12: Step discontinuity of a planar dielectric waveguide surrounded by the perfectly conducting electric walls with the inner PML. The whole structure is symmetric. L is the distance from the electric wall to the center. 34
Fig. 13: A plane wave perpendicularly incident into the PML region. 36
Fig. 14: Amplitude of reflection coefficient for incidence from waveguide A versus PML thickness for the planar step discontinuity (TE). $n_{core} = 2.236$, $n_{cladding} = 1.0$, $D = 0.2387\,\mu m$, $d = 0.2D$, $L = 3.2387\,\mu m$, and wavelength $\lambda = 1.5\,\mu m$ 37
Fig. 15: Amplitude of reflection coefficient for incidence from waveguide A versus the PML reflection coefficient R for the planar step discontinuity (TE). $n_{core} = 2.236$, $n_{cladding} = 1.0$, $D = 0.2387\,\mu m$, $d = 0.2D$, $L = 3.2387\,\mu m$, and wavelength $\lambda = 1.5\,\mu m$ 38
Fig. 16: Waveguide air gap. 43

Fig. 17: The cross-section for a rectangular dielectric waveguide enclosed by a perfectly conducting electric box with the inner PML. The waveguide core is located at the center of the whole structure. 44
Fig. 18: Power reflection coefficient versus the length of the waveguide air gap (quasi-TE). $D_x = 3.0\mu m$, $D_y = 2.0\mu m$, $L_x = 1.0\mu m$, $L_y = 0.5\mu m$, $n_{core} = 3.44$, $n_{cladding} = 3.39$, and wavelength $\lambda = 0.86\mu m$. 44
Fig. 19: Power transmission coefficient versus the length of the waveguide air gap (quasi-TE). $D_x = 3.0\mu m$, $D_y = 2.0\mu m$, $L_x = 1.0\mu m$, $L_y = 0.5\mu m$, $n_{core} = 3.44$, $n_{cladding} = 3.39$, and wavelength $\lambda = 0.86\mu m$. 45
Fig. 20: Power loss coefficient versus the length of the waveguide air gap (quasi-TE). $D_x = 3.0\mu m$, $D_y = 2.0\mu m$, $L_x = 1.0\mu m$, $L_y = 0.5\mu m$, $n_{core} = 3.44$, $n_{cladding} = 3.39$, and wavelength $\lambda = 0.86\mu m$ 45
Fig. 21: Power transmission coefficients versus the length of the waveguide air gap for different number of modes (quasi-TE). $D_x = 3.0\mu m$, $D_y = 2.0\mu m$, $L_x = 1.0\mu m$, $L_y = 0.5\mu m$, $n_{core} = 3.44$, $n_{cladding} = 3.39$, and wavelength $\lambda = 0.86\mu m$. 46
Fig. 22: Power reflection coefficient versus normalized core thickness for the waveguide facet (quasi-TE). $n_{core} = 3.6$, $n_{cladding} = 3.492$, $L_y = 0.5L_x$, and wavelength $\lambda = 0.86\mu m$ 47
Fig. 23: Top view of an asymmetric loaded rectangular waveguide. 48
Fig. 24: Cross-section of an asymmetric loaded rectangular waveguide. 49
Fig. 25: Electric field distributions of the fundamental quasi-TE mode for waveguide *C* (without loads) 50
Fig. 26: Electric field distributions of the fundamental quasi-TE mode for waveguide *A* in the asymmetric loaded rectangular waveguide. 50
Fig. 27: Electric field distributions of the fundamental quasi-TM mode for waveguide *A* in the asymmetric loaded rectangular waveguide. 51
Fig. 28: Mode power (DB) versus number of loads for the asymmetric loaded rectangular waveguide. 51

List of Tables

Table I: Coordinate stretching factors in the PML regions. 31
Table II: Complex propagation constants of the symmetric quasi-TE modes. Wavelength $\lambda = 1.064 \mu m$ and PML reflection coefficient $R = 10^{-8}$. 32
Table III: Comparison between the MMM and Rozzi's method for the planar step discontinuity (TE). PML reflection coefficient is 0.01. r_1 is the amplitude of reflection coefficient for incidence from waveguide A. The loss refers to incidence from waveguide A.....39

Chapter 1

Introduction

Waveguide structures with longitudinal discontinuities are involved in many applications. Analysis of the waveguide discontinuities is of great importance. A powerful approach is the mode matching method (MMM) with which the fields are described by a superposition of waveguide modes, and then the boundary conditions that the tangential fields in the cross-section of the waveguide structure must be continuous are imposed at the interface between different waveguide sections [1] [2] [3]. The method is inherently bi-directional and has been successfully applied for analysis of closed waveguides in which the mode spectrum is discrete. For open waveguide structures with infinite cross-sections, the mode spectrum includes the guided and radiation modes. The inclusion of the continuous radiation modes in the field expansion constitutes significant challenges for the applications of the MMM since usually a large number of sampled modes are needed to obtain reasonable results. The more difficult problem arises when we deal with three-dimensional (3D) waveguide structures with arbitrary transverse index profiles as the modes have to be calculated numerically. On the other hand, the radiation fields can also be represented approximately by summation of leaky modes [4]. Leaky modes, together with the guided modes, have been used in the modal expansion for analysis of many practical open waveguide structures. In principle, the leaky modes are the guided modes below cutoff, and they have complex propagation constants. It can be shown that the leaky modes can be used to approximate the portion of the radiation fields

near the core. The imaginary parts of the propagation constants for the leaky modes give rise to the attenuation coefficients which account for the leakage loss, and the modal field distributions close to the waveguide axis represent the radiation fields. It can be presented that the modal fields of the leaky modes diverge at infinity [4][5]. Fig. 1 shows the field divergence of two sample leaky modes (one sided and two sided) in a typical multilayer waveguide structure. We can see that the fields of the leaky modes do not obey the common orthogonality conditions as the integration needs to be performed over the infinite cross-section of the open waveguide structure. The unbounded modal field distributions and the mathematical difficulties make it tricky to apply the leaky modes in the modal expansion when defining modal orthogonality and normalization [4] [6].

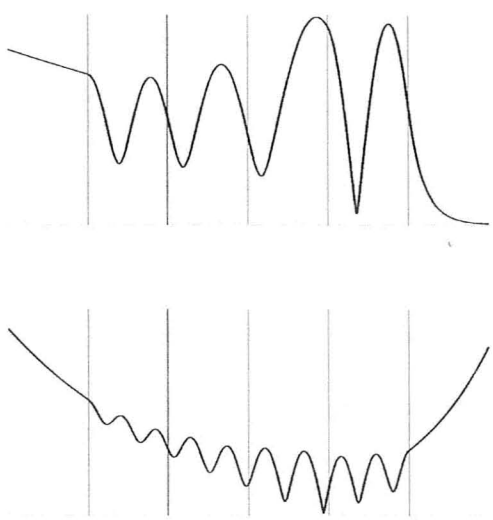

Fig. 1: Leaky waves in a multilayer waveguide.

The perfectly matched layer (PML) has been introduced for the truncation of the finite difference time domain (FDTD) lattices [7]. In practice, the PML is designed to surround the structure so that for any frequencies and angles of incidence, no reflection at the interface between non-PML and PML regions occurs. On the other hand, the PML backed by a perfectly conducting box can also be applied for analysis of waveguide problems. In this respect, the box with the inner PML encloses the waveguide structure in the transverse plane. We first consider the box without the inner PML. In this case, the mode spectrum is discrete and all the modes are on the axes in the propagation constant plane. The modes can be divided into two categories:

(1) Core-guided modes

The modes are confined to the core of the waveguide, and are approximately identical to the guided modes in the corresponding open waveguide if the perfectly conducting box is far away from the waveguide core.

(2) Box modes

The modes are related to the enclosing box, and the modal spectral spacing is inversely proportional to the size of the box.

Obviously, the size of the box without the inner PML should be sufficiently large in order to simulate the original open structure. Consequently, a large number of modes must be used in the field expansion. With the introduction of the inner PML as an absorbing boundary, the waves incident to the PML region would not be reflected and the closed waveguide structure can be seen as an open one [8]. As a result of the PML sandwiched between the guiding region and the perfectly conducting box enclosing the

computation domain, the mode spectrum is changed. Note that the size of the box is assumed to be large enough so that the guided modes of the original open waveguide structure would not be affected significantly. Now the entire mode spectrum is still discrete and includes the guided and complex modes, all of which are well defined and possess the normal mode characteristics such as the modal orthogonality and normalization. If the parameters of the PML are properly chosen, the complex modes can be used to represent the radiation fields in the modal expansion. It was demonstrated that the approach of the field expansion in terms of the guided and complex modes is more effective than the conventional approach. The approach has only been applied to two-dimensional (2D) waveguide structures with longitudinal discontinuities such as slab waveguide structures and 3D waveguide structures in which analytical modal solutions exist such as circular step index fibers [8] [9] [10]. In practice, the waveguide structures without analytical solutions are often encountered, such as a variety of specially shaped 3D waveguides. It is important to extend this approach to these 3D structures and therefore make the MMM a much more effective technique.

The guided and complex modes in a waveguide structure with an arbitrary transverse index profile surrounded by a perfectly conducting box with the inner PML can be calculated numerically by various methods. Among them, the finite difference (FD) method is an attractive technique. It is easy to program, and the matrix is sparse. In general, the waveguide modal analysis can be classified into three levels according to the mathematical complexity: scalar, semi-vectorial, and full-vectorial modal analyses [11] [12] [13]. Scalar modes are the solutions of the scalar wave equation, and the field

components and their first derivatives are continuous everywhere. For semi-vectorial modes, the modal fields are assumed to be predominantly linearly polarized so that only one major transverse field component needs to be considered, and the other transverse component is simply ignored. In the context of the full-vectorial approach, no field component is neglected. The full-vectorial wave governing equations are derived from Maxwell's equations without any approximation, and therefore the hybrid nature of the modal fields is fully considered. For many practical waveguide structures, however, the simplified semi-vectorial formulations can be used to calculate the modal fields with sufficient accuracy [14] [15].

In this thesis, we will investigate the effects of the key PML parameters on the accuracy and efficiency for the MMM in the context of the 2D waveguide structures with one-dimensional (1D) modes. A typical example is analyzed. Then we apply the method for analysis of the 3D arbitrary waveguide discontinuities with 2D modes based on the field expansion of the guided and complex modes. The 2D modes are computed by the semi or full-vectorial FD method. The thesis is organized as follows. Chapter 2 presents the main theoretical formulations including 1D and 2D modal governing equations. The effects of the PML parameters on the solutions are discussed in Chapter 3. Numerical results for 3D waveguide structures are given in Chapter 4. We conclude in Chapter 5.

Chapter 2

Formulations

In this Chapter, we will present the dispersion equations for 1D TE and TM modes in a 2D multilayer waveguide structure for which the transfer matrix method is used. Then the full-vectorial wave equations for 2D guided and complex modes in a 3D arbitrary waveguide structure enclosed by a perfectly conducting box coated by an anisotropic PML are obtained directly from Maxwell's equations. The transfer and scattering matrix formulations for single and multiple discontinuities are also given. For convenience, we make the following assumptions:

(1) The non-PML medium in the waveguide structure is isotropic, linear, and lossless.

(2) The permittivity and permeability of vacuum are denoted as ε_0 and μ_0, respectively. The permeability μ in the medium is equal to μ_0.

(3) ω and β are the angular frequency and the propagation constant, respectively.

(4) λ is the wavelength, and $k_0 = \dfrac{2\pi}{\lambda}$.

(5) The time dependency is expressed as $e^{j\omega t}$.

(6) The wave is propagating along z, and the z dependency is expressed as $e^{-j\beta z}$ which refers to the propagation in the positive z direction, or $e^{+j\beta z}$ in the negative z direction.

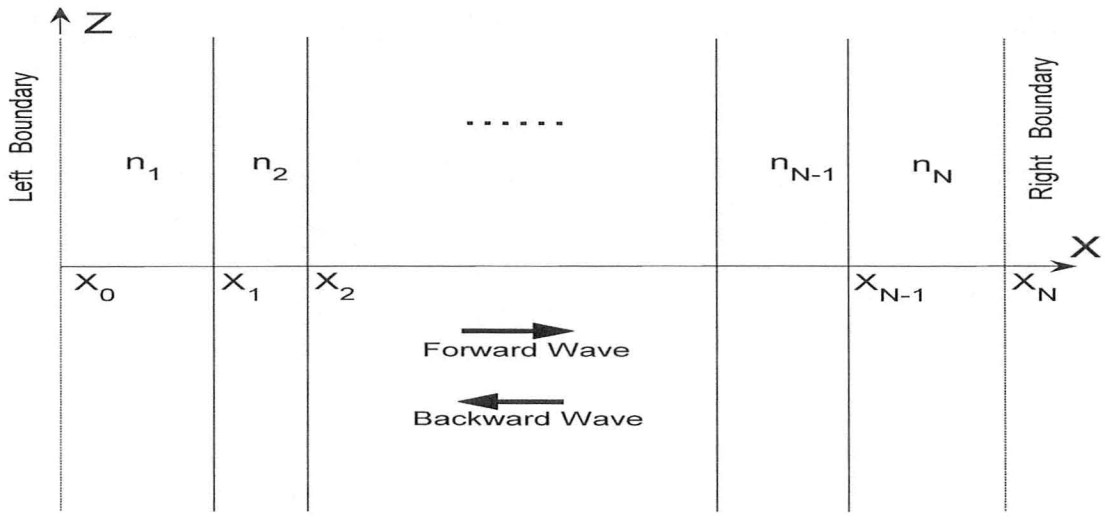

Fig. 2: A multilayer waveguide structure.

2.1 Modal Solutions

2.1.1 1D Multilayer Waveguide Modes

A general multilayer structure is shown in Fig. 2. There is no variation in y direction. n_m (m=1, 2, ..., N) is the refractive index of the m th layer and x_m is the position of the interface between the m th layer and the ($m+1$) th layer. The left and right artificial boundaries are inside the media with the refractive indices n_1 and n_N, respectively. Note that the artificial boundaries are employed here just for convenience. For instance, they are replaced by the perfectly conducting electric walls if the waveguide structure needs to be closed. For the open structure, they are simply removed. The modes can be classified as transverse electric modes (TE) which do not have the longitudinal electric field component, and transverse magnetic modes (TM) which do not have the longitudinal magnetic field component. For the 2D waveguide structure (1D modes), TE

modes have E_y, H_x, and H_z components; TM modes have H_y, E_x, and E_z components. We first consider TE modes. The field distribution (E_y) for TE modes in the m th layer can be written as [16]

$$E_y^{(m)}(x) = A_m \exp\left(-ik_x^{(m)}(x - x_m)\right) + B_m \exp\left(+ik_x^{(m)}(x - x_m)\right) \tag{2-1}$$

$$m = 1, 2, ..., N$$

where $k_x^{(m)} = \sqrt{k_0^2 n_m^2 - \beta^2}$. The other components H_x and H_z are given by

$$H_x^{(m)} = -\frac{\beta}{\omega\mu_0} E_y^{(m)} \tag{2-2}$$

and

$$H_z^{(m)} = j\frac{1}{\omega\mu_0}\frac{\partial E_y^{(m)}}{\partial x}. \tag{2-3}$$

Utilizing boundary conditions ($E_y^{(m)}$ and $\frac{\partial E_y^{(m)}}{\partial x}$ are continuous at the interface), the amplitudes of the plane wave components of the two neighboring layers for TE modes can be related as

$$\begin{bmatrix} A_m \\ B_m \end{bmatrix} = \frac{1}{2}\begin{bmatrix} (1+\frac{k_x^{(m+1)}}{k_x^{(m)}})e^{ik_x^{(m+1)}(x_{m+1}-x_m)} & (1-\frac{k_x^{(m+1)}}{k_x^{(m)}})e^{-ik_x^{(m+1)}(x_{m+1}-x_m)} \\ (1-\frac{k_x^{(m+1)}}{k_x^{(m)}})e^{ik_x^{(m+1)}(x_{m+1}-x_m)} & (1+\frac{k_x^{(m+1)}}{k_x^{(m)}})e^{-ik_x^{(m+1)}(x_{m+1}-x_m)} \end{bmatrix}\begin{bmatrix} A_{m+1} \\ B_{m+1} \end{bmatrix}. \tag{2-4}$$

Setting $U_m = A_m + B_m$ and $V_m = k_x^{(m)}(A_m - B_m)$, we obtain

$$\begin{bmatrix} U_m \\ V_m \end{bmatrix} = \begin{bmatrix} \cos k_x^{(m+1)}(x_{m+1} - x_m) & \frac{i}{k_x^{(m+1)}}\sin k_x^{(m+1)}(x_{m+1} - x_m) \\ ik_x^{(m+1)}\sin k_x^{(m+1)}(x_{m+1} - x_m) & \cos k_x^{(m+1)}(x_{m+1} - x_m) \end{bmatrix}\begin{bmatrix} U_{m+1} \\ V_{m+1} \end{bmatrix}. \tag{2-5}$$

Similar formulations can be derived for TM modes. We assume that the field distribution (H_y) for TM modes can be written as (2-1). E_x and E_z components are

$$E_x^{(m)} = \frac{\beta}{\omega\varepsilon_0 n_m^2} H_y^{(m)} \tag{2-6}$$

and

$$E_z^{(m)} = -j\frac{1}{\omega\varepsilon_0 n_m^2}\frac{\partial H_y^{(m)}}{\partial x}. \tag{2-7}$$

In this case, $H_y^{(m)}$ and $\frac{1}{n_m^2}\frac{\partial H_y^{(m)}}{\partial x}$ are continuous at the interface. We have for TM modes

$$\begin{bmatrix} A_m \\ B_m \end{bmatrix} = \frac{1}{2}\begin{bmatrix} (1+\frac{n_m^2}{n_{m+1}^2}\frac{k_x^{(m+1)}}{k_x^{(m)}})e^{ik_x^{(m+1)}(x_{m+1}-x_m)} & (1-\frac{n_m^2}{n_{m+1}^2}\frac{k_x^{(m+1)}}{k_x^{(m)}})e^{-ik_x^{(m+1)}(x_{m+1}-x_m)} \\ (1-\frac{n_m^2}{n_{m+1}^2}\frac{k_x^{(m+1)}}{k_x^{(m)}})e^{ik_x^{(m+1)}(x_{m+1}-x_m)} & (1+\frac{n_m^2}{n_{m+1}^2}\frac{k_x^{(m+1)}}{k_x^{(m)}})e^{-ik_x^{(m+1)}(x_{m+1}-x_m)} \end{bmatrix}\begin{bmatrix} A_{m+1} \\ B_{m+1} \end{bmatrix}. \tag{2-8}$$

Setting $U_m = A_m + B_m$ and $V_m = \frac{k_x^{(m)}}{n_m^2}(A_m - B_m)$, we obtain

$$\begin{bmatrix} U_m \\ V_m \end{bmatrix} = \begin{bmatrix} \cos k_x^{(m+1)}(x_{m+1}-x_m) & i\frac{n_{m+1}^2}{k_x^{(m+1)}}\sin k_x^{(m+1)}(x_{m+1}-x_m) \\ i\frac{k_x^{(m+1)}}{n_{m+1}^2}\sin k_x^{(m+1)}(x_{m+1}-x_m) & \cos k_x^{(m+1)}(x_{m+1}-x_m) \end{bmatrix}\begin{bmatrix} U_{m+1} \\ V_{m+1} \end{bmatrix}. \tag{2-9}$$

In the PML region, the real thickness $d_{m+1} = x_{m+1} - x_m$ in the above formulations should be replaced by the complex one $\tilde{d}_{m+1} = \tilde{x}_{m+1} - \tilde{x}_m$ [17]. The complex thickness is given by

$$\tilde{d}_{m+1} = \tilde{x}_{m+1} - \tilde{x}_m = \int_{x_m}^{x_{m+1}} s_x dx \tag{2-10}$$

where s_x, called the coordinate-stretching factor, is complex in the PML region. We can relate the amplitudes of the plane wave components by using a total matrix as follows

$$\begin{bmatrix} A_0 \\ B_0 \end{bmatrix} = \begin{bmatrix} M_{11} & M_{12} \\ M_{21} & M_{22} \end{bmatrix} \begin{bmatrix} A_N \\ B_N \end{bmatrix}. \tag{2-11}$$

Alternatively, we may write

$$\begin{bmatrix} U_0 \\ V_0 \end{bmatrix} = \begin{bmatrix} T_{11} & T_{12} \\ T_{21} & T_{22} \end{bmatrix} \begin{bmatrix} U_N \\ V_N \end{bmatrix}. \tag{2-12}$$

For the guided waves, the fields must vanish at infinity. Setting $A_0 = B_N = 0$, we have the following dispersion equation

$$M_{11} = 0. \tag{2-13}$$

Note that the above dispersion equation can also be used for leaky mode calculation. If the left and right boundaries are replaced by the perfectly conducting electric walls, we can use the condition that the tangential electric field must vanish at the electric walls, and obtain

$$T_{12} = 0 \tag{2-14}$$

for TE modes, and

$$T_{21} = 0 \tag{2-15}$$

for TM modes.

With the presence of the PML, we need to find the complex roots. A method for solving the above dispersion equations is called the argument principle method (APM) [18] [19] [20], which can be utilized to search for the zeros of any analytic function in the complex plane (See Appendix A). The method produces a polynomial, the zeros of which

coincide with the zeros of the original function. However, the method would cause numerical inaccuracy in some cases. Another method (See Appendix B) is quite simple. Starting out from the structure without the inner PML, we can easily find the discrete modes, which are located on the coordinate axes. Then we gradually increase the attenuation in the PML, and track the modes as they move into the complex plane. In general, the method works well, but it is time consuming if the attenuation is very large.

2.1.2 2D Waveguide Modes

We consider a waveguide structure where the transverse index profile $n(x, y)$ is arbitrary and defined in the Cartesian coordinate system. The waveguide structure is surrounded by an anisotropic PML backed by a perfectly conducting electric box (See Fig. 3). The box is assumed to be far away from the waveguide core so that the guided modes in the original open waveguide structure are not affected significantly. We need to derive the full-vectorial wave equations. The Maxwell's equations in the non-PML and PML regions can be written as

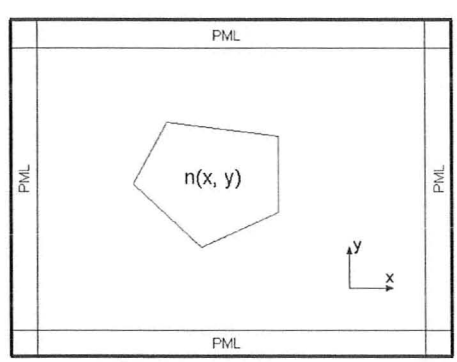

Fig. 3: A 2D arbitrary waveguide structure surrounded by a perfectly conducting electric box with the inner PML.

$$\nabla \times \vec{E} = -j\omega\mu_0 [\Lambda] \vec{H} \tag{2-16a}$$

$$\nabla \times \vec{H} = j\omega\varepsilon_0 n^2 [\Lambda] \vec{E} \tag{2-16b}$$

Where $[\Lambda]$ is given by [21]

$$[\Lambda] = \begin{bmatrix} \frac{s_y}{s_x} & 0 & 0 \\ 0 & \frac{s_x}{s_y} & 0 \\ 0 & 0 & s_x s_y \end{bmatrix}. \tag{2-17}$$

The coordinate-stretching factor s_k is the function of k only [17], where $k = x, y$. In the non-PML region, $s_x = s_y = 1$; in the PML region, s_x and s_y are complex and can be written as

$$s_x = \kappa_x - j\frac{\sigma_x}{\omega\varepsilon_0 n^2} \tag{2-18a}$$

$$s_y = \kappa_y - j\frac{\sigma_y}{\omega\varepsilon_0 n^2}. \tag{2-18b}$$

From the Maxwell's equations (2-16), we can obtain the following vector wave equation for the electric field

$$\nabla \times \left([\Lambda]^{-1} \nabla \times \vec{E} \right) = \omega^2 \mu_0 \varepsilon_0 n^2 [\Lambda] \vec{E}. \tag{2-19}$$

Utilizing

$$\vec{E} = \vec{E}_t + E_z \hat{z} \tag{2-20}$$

$$\nabla = \nabla_t + \frac{\partial}{\partial z}\hat{z} \tag{2-21}$$

$$\nabla \times \vec{E} = \nabla_t \times \vec{E}_t + \nabla_t \times (E_z \hat{z}) - j\beta \hat{z} \times \vec{E}_t \tag{2-22}$$

where $\hat{z}$ is the unit vector along z, $\vec{E}_t$ is the transverse electric vector, and E_z is the longitudinal electric component, we have

$$\begin{aligned} &\nabla_t \times \left(\frac{1}{s_x s_y} \nabla_t \times \vec{E}_t \right) + \hat{z} \times \left[[\Lambda]_T^{-1} \nabla_t \times (-j\beta E_z \hat{z}) \right] \\ &- \beta^2 \hat{z} \times \left([\Lambda]_T^{-1} \hat{z} \times \vec{E}_t \right) = \omega^2 \mu_0 \varepsilon_0 n^2 [\Lambda]_T \vec{E}_t \end{aligned} \tag{2-23}$$

where

$$[\Lambda]_T = \begin{bmatrix} \frac{s_y}{s_x} & 0 \\ 0 & \frac{s_x}{s_y} \end{bmatrix}. \tag{2-24}$$

From $\nabla \cdot \vec{D} = \nabla \cdot \left(\varepsilon_0 n^2 [\Lambda] \vec{E} \right) = 0$, we obtain

$$E_z = \frac{\nabla_t \cdot \left(n^2 [\Lambda]_T \vec{E}_t \right)}{j\beta n^2 s_x s_y}. \tag{2-25}$$

Substituting (2-25) into (2-23), we obtain the following full-vectorial wave equation for the transverse electric fields

$$\begin{aligned} &\nabla_t \times \left(\frac{1}{s_x s_y} \nabla_t \times \vec{E}_t \right) - \hat{z} \times \left[[\Lambda]_T^{-1} \nabla_t \times \left(\frac{\nabla_t \cdot (n^2 [\Lambda]_T \vec{E}_t)}{n^2 s_x s_y} \hat{z} \right) \right] \\ &- \beta^2 \hat{z} \times \left([\Lambda]_T^{-1} \hat{z} \times \vec{E}_t \right) = \omega^2 \mu_0 \varepsilon_0 n^2 [\Lambda]_T \vec{E}_t . \end{aligned} \tag{2-26}$$

The full-vectorial wave equations for E_x and E_y in the Cartesian coordinate system can be written as

$$\frac{1}{s_x}\frac{\partial}{\partial x}\left[\frac{1}{n^2}\frac{1}{s_x}\frac{\partial}{\partial x}\left(n^2\frac{1}{s_x}E_x\right)\right]+\frac{1}{s_y}\frac{\partial}{\partial y}\left[\frac{1}{s_y}\frac{\partial}{\partial y}\left(\frac{1}{s_x}E_x\right)\right]+k_0^2n^2\frac{1}{s_x}E_x$$
$$+\frac{1}{s_x}\frac{\partial}{\partial x}\left[\frac{1}{n^2}\frac{1}{s_y}\frac{\partial}{\partial y}\left(n^2\frac{1}{s_y}E_y\right)\right]-\frac{1}{s_y}\frac{\partial}{\partial y}\left[\frac{1}{s_x}\frac{\partial}{\partial x}\left(\frac{1}{s_y}E_y\right)\right]=\beta^2\frac{1}{s_x}E_x \tag{2-27}$$

and

$$\frac{1}{s_y}\frac{\partial}{\partial y}\left[\frac{1}{n^2}\frac{1}{s_y}\frac{\partial}{\partial y}\left(n^2\frac{1}{s_y}E_y\right)\right]+\frac{1}{s_x}\frac{\partial}{\partial x}\left[\frac{1}{s_x}\frac{\partial}{\partial x}\left(\frac{1}{s_y}E_y\right)\right]+k_0^2n^2\frac{1}{s_y}E_y$$
$$+\frac{1}{s_y}\frac{\partial}{\partial y}\left[\frac{1}{n^2}\frac{1}{s_x}\frac{\partial}{\partial x}\left(n^2\frac{1}{s_x}E_x\right)\right]-\frac{1}{s_x}\frac{\partial}{\partial x}\left[\frac{1}{s_y}\frac{\partial}{\partial y}\left(\frac{1}{s_x}E_x\right)\right]=\beta^2\frac{1}{s_y}E_y \tag{2-28}$$

where $k_0=\omega\sqrt{\mu_0\varepsilon_0}$. Solving the above equations (2-27) and (2-28) with proper boundary conditions, we can obtain the full-vectorial modal solutions. The transverse magnetic field components H_x and H_y can be readily obtained from the Maxwell's equations by the following expressions in terms of the transverse electric field components

$$H_x=-\frac{\beta}{\omega\mu_0}\frac{s_x}{s_y}E_y+\frac{1}{\beta\omega\mu_0}\frac{s_x}{s_y}\frac{\partial}{\partial y}\left[\frac{1}{n^2}\frac{1}{s_y}\frac{\partial}{\partial y}\left(n^2\frac{1}{s_y}E_y\right)\right]$$
$$+\frac{1}{\beta\omega\mu_0}\frac{s_x}{s_y}\frac{\partial}{\partial y}\left[\frac{1}{n^2}\frac{1}{s_x}\frac{\partial}{\partial x}\left(n^2\frac{1}{s_x}E_x\right)\right] \tag{2-29}$$

and

$$H_y=\frac{\beta}{\omega\mu_0}\frac{s_y}{s_x}E_x-\frac{1}{\beta\omega\mu_0}\frac{s_y}{s_x}\frac{\partial}{\partial x}\left[\frac{1}{n^2}\frac{1}{s_x}\frac{\partial}{\partial x}\left(n^2\frac{1}{s_x}E_x\right)\right]$$
$$-\frac{1}{\beta\omega\mu_0}\frac{s_y}{s_x}\frac{\partial}{\partial x}\left[\frac{1}{n^2}\frac{1}{s_y}\frac{\partial}{\partial y}\left(n^2\frac{1}{s_y}E_y\right)\right]. \tag{2-30}$$

Under the semi-vectorial approximation, we assume that only one dominant transverse electric component exists for the quasi-TE and quasi-TM modes, respectively. For convenience, we write the semi-vectorial governing equations as follows

$$\frac{1}{s_x}\frac{\partial}{\partial x}\left[\frac{1}{n^2}\frac{1}{s_x}\frac{\partial}{\partial x}\left(n^2\frac{1}{s_x}E_x\right)\right]+\frac{1}{s_y}\frac{\partial}{\partial y}\left[\frac{1}{s_y}\frac{\partial}{\partial y}\left(\frac{1}{s_x}E_x\right)\right] + k_0^2 n^2\frac{1}{s_x}E_x = \beta^2\frac{1}{s_x}E_x \tag{2-31}$$

and

$$H_y = \frac{\beta}{\omega\mu_0}\frac{s_y}{s_x}E_x - \frac{1}{\beta\omega\mu_0}\frac{s_y}{s_x}\frac{\partial}{\partial x}\left[\frac{1}{n^2}\frac{1}{s_x}\frac{\partial}{\partial x}\left(n^2\frac{1}{s_x}E_x\right)\right] \tag{2-32}$$

for the quasi-TE modes where $E_y = 0$;

$$\frac{1}{s_y}\frac{\partial}{\partial y}\left[\frac{1}{n^2}\frac{1}{s_y}\frac{\partial}{\partial y}\left(n^2\frac{1}{s_y}E_y\right)\right]+\frac{1}{s_x}\frac{\partial}{\partial x}\left[\frac{1}{s_x}\frac{\partial}{\partial x}\left(\frac{1}{s_y}E_y\right)\right] + k_0^2 n^2\frac{1}{s_y}E_y = \beta^2\frac{1}{s_y}E_y \tag{2-33}$$

and

$$H_x = -\frac{\beta}{\omega\mu_0}\frac{s_x}{s_y}E_y + \frac{1}{\beta\omega\mu_0}\frac{s_x}{s_y}\frac{\partial}{\partial y}\left[\frac{1}{n^2}\frac{1}{s_y}\frac{\partial}{\partial y}\left(n^2\frac{1}{s_y}E_y\right)\right] \tag{2-34}$$

for the quasi-TM modes where $E_x = 0$.

2.2 Mode Matching Solutions

In a waveguide structure surrounded by a perfectly conducting box with an inner anisotropic PML, the mode spectrum includes guided and complex modes. These complex modes which depend on the PML parameters, together with guided modes, are

to be utilized in the modal expansion for the closed waveguide structure. We consider a single waveguide discontinuity where two waveguides (A and B) of different transverse configuration are jointed at the position $z = 0$. N modes in waveguide A and M modes in waveguide B are to be included in the modal expansion. Fig. 4 shows the structure formed by waveguide A and B. The transverse electric and magnetic fields ($\vec{E}_t$ and $\vec{H}_t$) in waveguide A and B in the Cartesian coordinate system can be written as

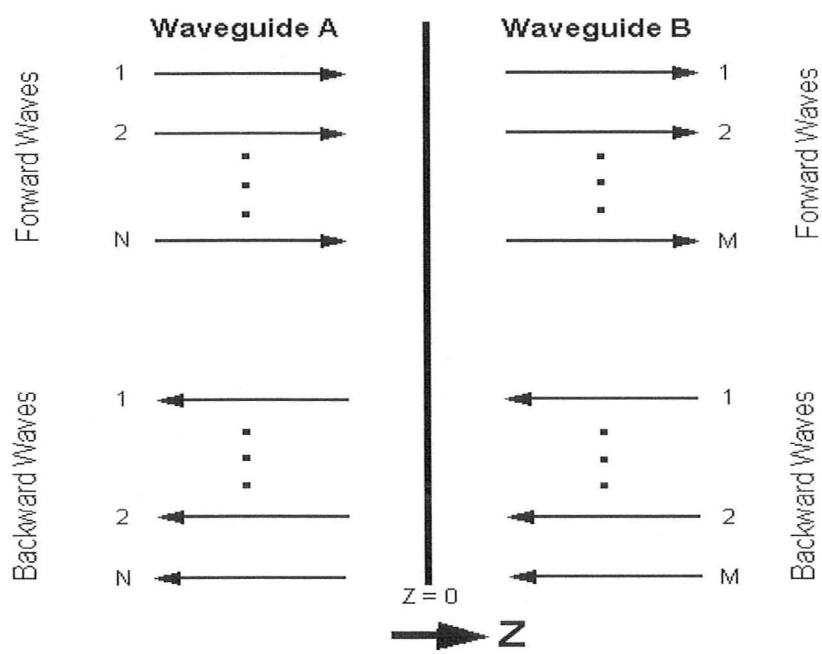

Fig. 4: A waveguide discontinuity.

$$\vec{E}_t^A(x,y,z) = \sum_{n=1}^{N} (a_n^+ e^{-j\beta_n^A z} + a_n^- e^{j\beta_n^A z}) \vec{e}_{tn}^A(x,y) \tag{2-35a}$$

$$\vec{H}_t^A(x,y,z) = \sum_{n=1}^{N} (a_n^+ e^{-j\beta_n^A z} - a_n^- e^{j\beta_n^A z}) \vec{h}_{tn}^A(x,y) \tag{2-35b}$$

$$\vec{E}_t^B(x,y,z) = \sum_{m=1}^{M}(b_m^+ e^{-j\beta_m^B z} + b_m^- e^{j\beta_m^B z})\vec{e}_{tm}^B(x,y) \tag{2-36a}$$

$$\vec{H}_t^B(x,y,z) = \sum_{m=1}^{M}(b_m^+ e^{-j\beta_m^B z} - b_m^- e^{j\beta_m^B z})\vec{h}_{tm}^B(x,y) \tag{2-36b}$$

where t denotes the transverse component, β_n^A is the propagation constant of the nth mode, $\vec{e}_{tn}^A$ and $\vec{h}_{tn}^A$ are the transverse electric and magnetic vectors of the nth mode, respectively, and a_n^+ and a_n^- are the amplitudes of forward and backward waves of the nth mode, respectively. They are defined for waveguide A. The notations for waveguide B are defined similarly. Utilizing the boundary condition at the interface, we have

$$\sum_{n=1}^{N}(a_n^+ + a_n^-)\vec{e}_{tn}^A(x,y) = \sum_{m=1}^{M}(b_m^+ + b_m^-)\vec{e}_{tm}^B(x,y) \tag{2-37}$$

$$\sum_{n=1}^{N}(a_n^+ - a_n^-)\vec{h}_{tn}^A(x,y) = \sum_{m=1}^{M}(b_m^+ - b_m^-)\vec{h}_{tm}^B(x,y)\,. \tag{2-38}$$

Take the cross product with $\vec{h}_{tk}^B$ and $\vec{e}_{tk}^B$, respectively, and integrate over the waveguide cross-section S, we obtain

$$\sum_{n=1}^{N}(a_n^+ + a_n^-) < \vec{e}_{tn}^A, \vec{h}_{tk}^B > = \sum_{m=1}^{M}(b_m^+ + b_m^-) < \vec{e}_{tm}^B, \vec{h}_{tk}^B > \tag{2-39}$$

$$\sum_{n=1}^{N}(a_n^+ - a_n^-) < \vec{e}_{tk}^B, \vec{h}_{tn}^A > = \sum_{m=1}^{M}(b_m^+ - b_m^-) < \vec{e}_{tk}^B, \vec{h}_{tm}^B > \tag{2-40}$$

where the inner product of the field vectors is given by

$$< \vec{e}, \vec{h} > = \frac{1}{2}\iint_S (\vec{e} \times \vec{h}) \cdot \hat{z}\, ds\,. \tag{2-41}$$

With the use of the following orthogonality relation between the modes

$$< \vec{e}_{tm}, \vec{h}_{tn} >= \frac{1}{2} \iint_S (\vec{e}_{tm} \times \vec{h}_{tn}) \cdot \hat{z}\, ds =< \vec{e}_{tm}, \vec{h}_{tm} > \delta_{mn}, \tag{2-42}$$

we obtain

$$b_m^+ = \sum_{n=1}^{N} a_n^+ \left[\frac{< \vec{e}_{tn}^{\,A}, \vec{h}_{tm}^{\,B} > + < \vec{e}_{tm}^{\,B}, \vec{h}_{tn}^{\,A} >}{2 < \vec{e}_{tm}^{\,B}, \vec{h}_{tm}^{\,B} >} \right] + \sum_{n=1}^{N} a_n^- \left[\frac{< \vec{e}_{tn}^{\,A}, \vec{h}_{tm}^{\,B} > - < \vec{e}_{tm}^{\,B}, \vec{h}_{tn}^{\,A} >}{2 < \vec{e}_{tm}^{\,B}, \vec{h}_{tm}^{\,B} >} \right] \tag{2-43a}$$

$$b_m^- = \sum_{n=1}^{N} a_n^+ \left[\frac{< \vec{e}_{tn}^{\,A}, \vec{h}_{tm}^{\,B} > - < \vec{e}_{tm}^{\,B}, \vec{h}_{tn}^{\,A} >}{2 < \vec{e}_{tm}^{\,B}, \vec{h}_{tm}^{\,B} >} \right] + \sum_{n=1}^{N} a_n^- \left[\frac{< \vec{e}_{tn}^{\,A}, \vec{h}_{tm}^{\,B} > + < \vec{e}_{tm}^{\,B}, \vec{h}_{tn}^{\,A} >}{2 < \vec{e}_{tm}^{\,B}, \vec{h}_{tm}^{\,B} >} \right] \tag{2-43b}$$

where we have used the subscript m instead of k, and the coefficients b_m^+ and b_m^- are the amplitudes of forward and backward waves of the mth mode in waveguide B, respectively. In the matrix form, we have

$$\begin{bmatrix} B^+ \\ B^- \end{bmatrix} = \begin{bmatrix} b_1^+ \\ b_2^+ \\ . \\ b_M^+ \\ b_1^- \\ b_2^- \\ . \\ b_M^- \end{bmatrix} = \left[T_{junction} \right] \begin{bmatrix} a_1^+ \\ a_2^+ \\ . \\ a_N^+ \\ a_1^- \\ a_2^- \\ . \\ a_N^- \end{bmatrix} = \left[T_{junction} \right] \begin{bmatrix} A^+ \\ A^- \end{bmatrix}. \tag{2-44}$$

The transfer matrix for n modes in a uniform waveguide section is given by

$$\left[T_{uniform\ \ section} \right] = \begin{bmatrix} e^{-j\beta_1 d} & & & & & & & \\ & e^{-j\beta_2 d} & & & & & & \\ & & . & & & & & \\ & & & e^{-j\beta_n d} & & & & \\ & & & & e^{+j\beta_1 d} & & & \\ & & & & & e^{+j\beta_2 d} & & \\ & & & & & & . & \\ & & & & & & & e^{+j\beta_n d} \end{bmatrix} \tag{2-45}$$

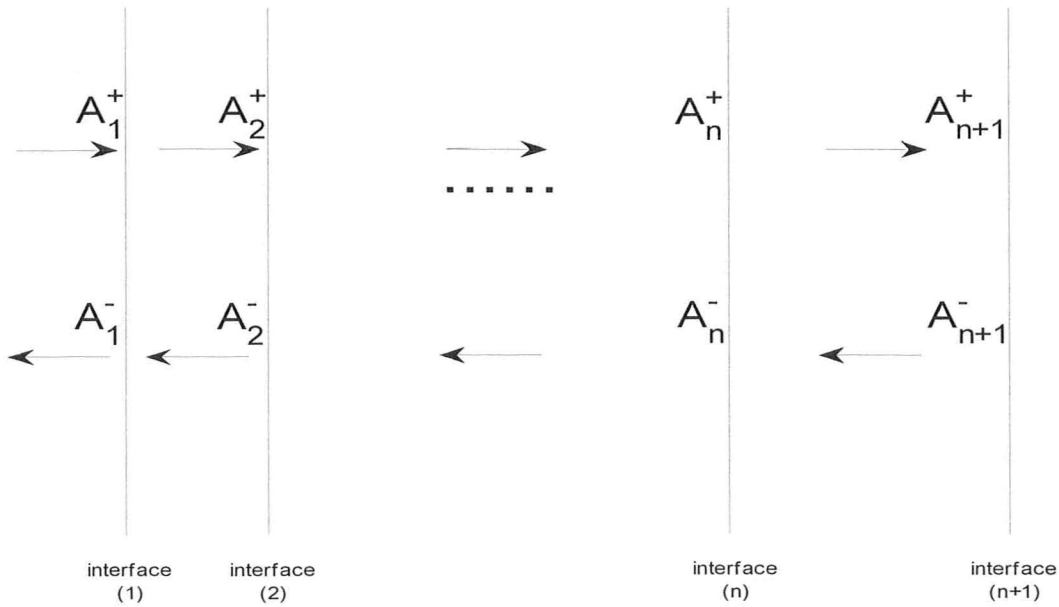

Fig. 5: Multiple waveguide discontinuities.

where d is the length of the waveguide section, and the values of the non-diagonal elements are zeros. For multiple discontinuities along the waveguide axis, the transfer or scattering matrix formulations can be utilized to connect the modal amplitudes of the different sections [22] [23].

2.3 Multiple Waveguide Discontinuities

We consider multiple waveguide discontinuities shown in Fig. 5. The notations A_1^+, A_1^-, A_2^+, A_2^- ... A_n^+, A_n^-, A_{n+1}^+, A_{n+1}^- represent the values of the forward and backward waves at the left sides of the 1th, 2th, ..., nth, and (n+1)th discontinuities, respectively. For the first discontinuity, we can write T and S matrix formulations as

$$\begin{bmatrix} A_2^+ \\ A_2^- \end{bmatrix} = \left[T^1_{matrix}\right] \begin{bmatrix} A_1^+ \\ A_1^- \end{bmatrix} \tag{2-46}$$

and

$$\begin{bmatrix} A_2^+ \\ A_1^- \end{bmatrix} = \left[S^1_{matrix}\right] \begin{bmatrix} A_1^+ \\ A_2^- \end{bmatrix} = \begin{bmatrix} T_{1,2} & R_{2,1} \\ R_{1,2} & T_{2,1} \end{bmatrix} \begin{bmatrix} A_1^+ \\ A_2^- \end{bmatrix}. \tag{2-47}$$

Note that we have included the contribution of the uniform section (invariant along the propagation direction) to the above T and S matrices. Further we can write

$$\begin{bmatrix} A_{n+1}^+ \\ A_{n+1}^- \end{bmatrix} = \left[T^n_{matrix}\right]\left[T^{n-1}_{matrix}\right]\ldots\left[T^1_{matrix}\right] \begin{bmatrix} A_1^+ \\ A_1^- \end{bmatrix} \tag{2-48}$$

Given

$$\begin{bmatrix} A_n^+ \\ A_1^- \end{bmatrix} = \begin{bmatrix} T_{1,n} & R_{n,1} \\ R_{1,n} & T_{n,1} \end{bmatrix} \begin{bmatrix} A_1^+ \\ A_n^- \end{bmatrix} \tag{2-49}$$

and

$$\begin{bmatrix} A_{n+1}^+ \\ A_n^- \end{bmatrix} = \begin{bmatrix} T_{n,n+1} & R_{n+1,n} \\ R_{n,n+1} & T_{n+1,n} \end{bmatrix} \begin{bmatrix} A_n^+ \\ A_{n+1}^- \end{bmatrix} \tag{2-50}$$

We can obtain

$$\begin{bmatrix} A_{n+1}^+ \\ A_1^- \end{bmatrix} = \begin{bmatrix} T_{1,n+1} & R_{n+1,1} \\ R_{1,n+1} & T_{n+1,1} \end{bmatrix} \begin{bmatrix} A_1^+ \\ A_{n+1}^- \end{bmatrix} \tag{2-51}$$

where

$$\begin{aligned} T_{1,n+1} &= T_{n,n+1}(I - R_{n,1}R_{n,n+1})^{-1}T_{1,n} \\ R_{n+1,1} &= T_{n,n+1}(I - R_{n,1}R_{n,n+1})^{-1}R_{n,1}T_{n+1,n} + R_{n+1,n} \\ R_{1,n+1} &= T_{n,1}(I - R_{n,n+1}R_{n,1})^{-1}R_{n,n+1}T_{1,n} + R_{1,n} \\ T_{n+1,1} &= T_{n,1}(I - R_{n,n+1}R_{n,1})^{-1}T_{n+1,n} \end{aligned} \tag{2-52}$$

Appendix A: 1D Mode Calculation and Mode Matching

The purpose is to find the zeros of the dispersion equation. If the modes are complex, the roots must be searched for in the complex plane. It can be numerically challenging especially when a large number of zeros need to be found. Two common approaches are presented below.

A.1 Argument Principle Method (APM)

APM is a mathematical technique and can be used to find the zeros of any analytical function in the complex plane. With APM, we need to numerically compute the contour integral

$$s_m = \frac{1}{2\pi i}\oint_C z^m \frac{f'(z)}{f(z)}dz = \sum_{j=1}^{n} z_j^m \tag{2-53}$$

where $f(z)$ is an analytical function, and $z_1, z_2, ..., z_n$ are n zeros of $f(z)$ inside the contour C. The derivative of $f(z)$ can be calculated by

$$\begin{aligned} f'(z_0) &= \frac{1}{2\pi i}\oint_c \frac{f(z)}{(z-z_0)^2}dz \\ &= \int_0^1 \frac{f(z_0 + Re^{i2\pi t})}{Re^{i2\pi t}}dt \\ &\approx \frac{1}{N}\sum_{m=1}^{N} \frac{f(z_0 + Re^{i2\pi \frac{m}{N}})}{Re^{i2\pi \frac{m}{N}}} \end{aligned} \tag{2-54}$$

where R is the radius of the circle. A polynomial which has the same roots as the function $f(z)$ can be formed, and it is given by

$$p(z) = \sum_{k=0}^{n} c_k z^k \tag{2-55}$$

where

$$\begin{aligned}
&c_n = 1 \\
&c_{n-1} + s_1 c_n = 0 \\
&2c_{n-2} + s_1 c_{n-1} + s_2 c_n = 0 \\
&\ldots\ldots \\
&(n-1)c_1 + s_1 c_2 + s_2 c_3 + \ldots + s_{n-1} c_n = 0 \\
&nc_0 + s_1 c_1 + s_2 c_2 + \ldots + s_n c_n = 0.
\end{aligned} \tag{2-56}$$

As the integrals are computed numerically, the final refinement usually needs to be done by root searching techniques such as the Newton's method

$$z_{k+1} = z_k - \frac{f(z_k)}{f'(z_k)}. \tag{2-57}$$

The basic procedure for APM is summarized as follows

(1) Calculate the number of zeros of $f(z)$ in a region *D*. If *D* contains too many zeros, divide *D* into smaller regions *D1, D2*, ... The number of zeros in each region usually should be less than 5 so that the root searching technique for the polynomial is more efficient.

(2) For each region, calculate s_1, s_2, ..., and s_k, where *k* is the number of zeros in the region.

(3) Calculate the coefficients of the polynomial $p(z)$.

(4) Calculate the roots of the polynomial $p(z)$, which are initial values for further refinement.

(5) Applying the Newton's method with the initial conditions to the original function $f(z)$.

A.2 Smooth Transition Method

The modes in a 1D waveguide surrounded by perfectly conducting electric walls are located on the axes in the complex plane, and they can be found easily. When we gradually increase the value of the specified parameter, the modes would move away from the axes and can be tracked by numerical techniques (e.g. Newton's method). The specified parameter depends on the problems. For instance, if we want to calculate the leaky modes, the initial value of the parameter represents the closed waveguide and the final value indicates that the waveguide becomes open. For the complex modes with the presence of the PML, the specified parameter is the attenuation coefficient in the PML region. In this respect, the initial value of the parameter represents the absence of the PML, and all the modes are on the axes.

A.3 Application

A typical double-layer antireflection coated facet [24], shown in Fig. 6, will be analyzed by the MMM. The whole waveguide structure is enclosed by two perfectly conducting electric walls with the inner PML. In the case, the power reflection coefficients are expected to be very small.

In order to calculate the reflectivity in the double-layer antireflection coated facet, we need to find the eigenmodes for four different waveguides: one symmetric slab waveguide and three uniform waveguides. These eigenmodes can be computed by the smooth transition method. For this case, the coordinate stretching factor is set constant in the PML region. The calculated normalized propagation constants for the symmetric slab

waveguide are shown in Fig. 7. It can be seen that the original box modes on the axes move into the complex plane as the attenuation is added in the PML region.

The mode matching formulations involve the overlap integrals which can be obtained analytically. For instance, the overlap integrals for TE modes can be written as

$$< e_t, h_t >= \frac{1}{2}\int_{x_0}^{x_n} -E_y H_x dx = \int_{x_0}^{x_n} \frac{\beta}{2\omega\mu_0} E_y^2 dx \tag{2-58a}$$

$$< e_t^A, h_t^B >= \frac{1}{2}\int_{x_0}^{x_n} E_y^A \frac{\beta^B}{\omega\mu_0} E_y^B dx = \frac{\beta^B}{2\omega\mu_0}\int_{x_0}^{x_n} E_y^A E_y^B dx \tag{2-58b}$$

$$< e_t^B, h_t^A >= \frac{1}{2}\int_{x_0}^{x_n} E_y^B \frac{\beta^A}{\omega\mu_0} E_y^A dx = \frac{\beta^A}{2\omega\mu_0}\int_{x_0}^{x_n} E_y^A E_y^B dx \tag{2-58c}$$

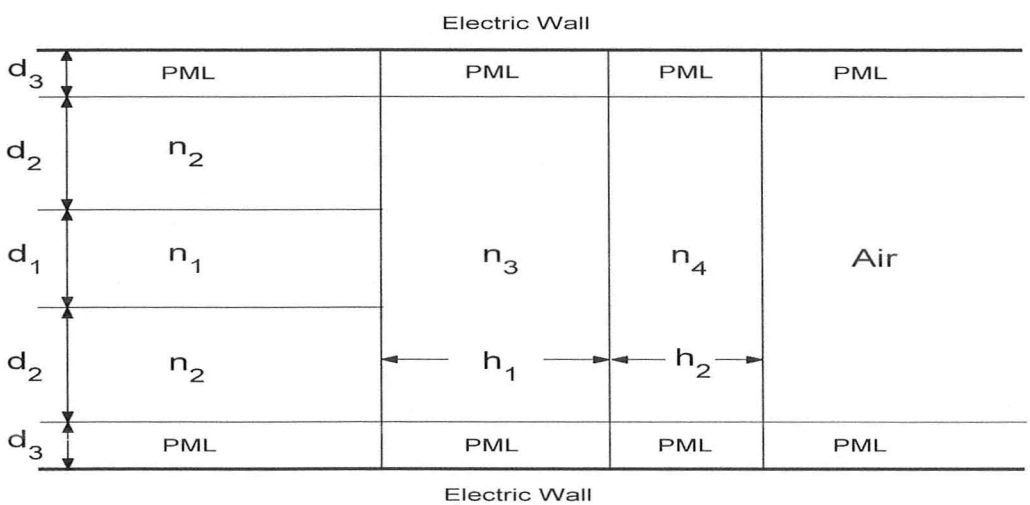

Fig. 6: A typical double-layer antireflection coated facet. $n_1 = 3.524$, $n_2 = 3.17$, $n_3 = 1.82$, $n_4 = 1.65$, $d_1 = 0.11\,\mu m$, $d_2 = 3.6\,\mu m$, $d_3 = 0.5\,\mu m$, $h_1 = 0.1816\,\mu m$, and wavelength $\lambda = 1.54\,\mu m$.

where x_0 and x_n are the coordinates of two end points, respectively. The electric walls with the PML are located where the amplitude of the guided mode in the symmetric slab waveguide is sufficiently small. As we have multiple discontinuities, *S* matrix cascade is to be used to connect the fields in different waveguide sections. Fig. 8 shows the dependence of the power reflection coefficients of the double-layer antireflection coated facet on the second layer film thickness. The total of 50 modes are used in the mode expansion. It can be seen that there is one minimum point for the power reflection coefficients, which occurs at $h_2 \approx 0.05\,\mu m$.

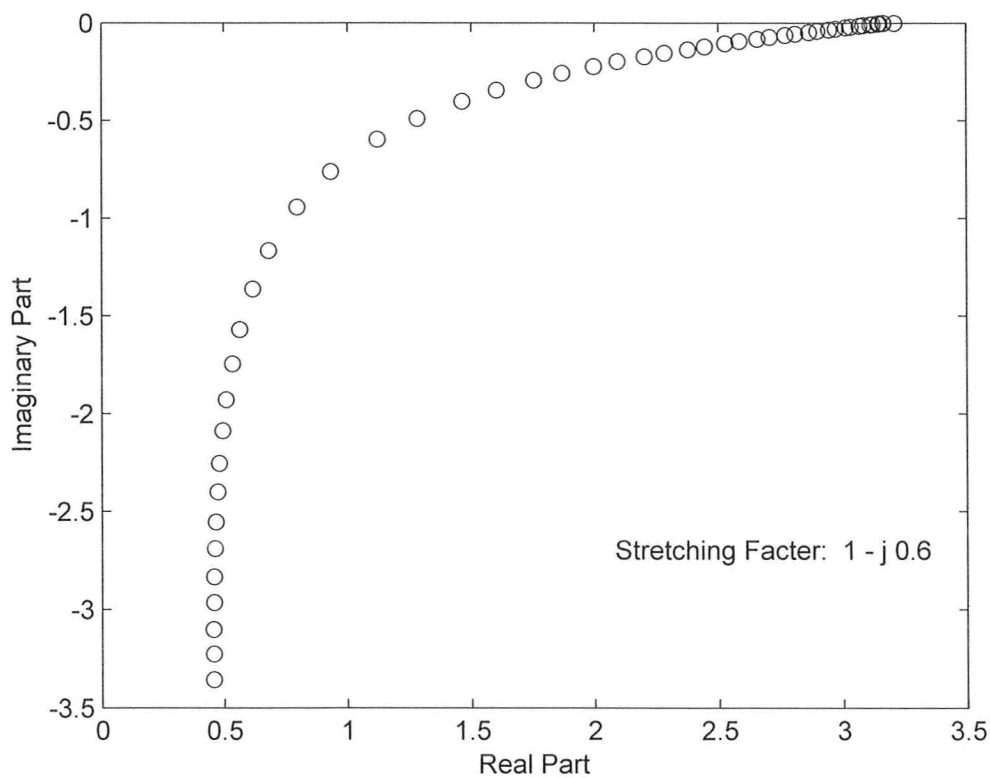

Fig. 7: Normalized propagation constants for the slab waveguide in a typical double-layer antireflection coated facet (TE). $n_1 = 3.524$, $n_2 = 3.17$, $d_1 = 0.11\,\mu m$, $d_2 = 3.6\,\mu m$, $d_3 = 0.5\,\mu m$, and wavelength $\lambda = 1.54\,\mu m$.

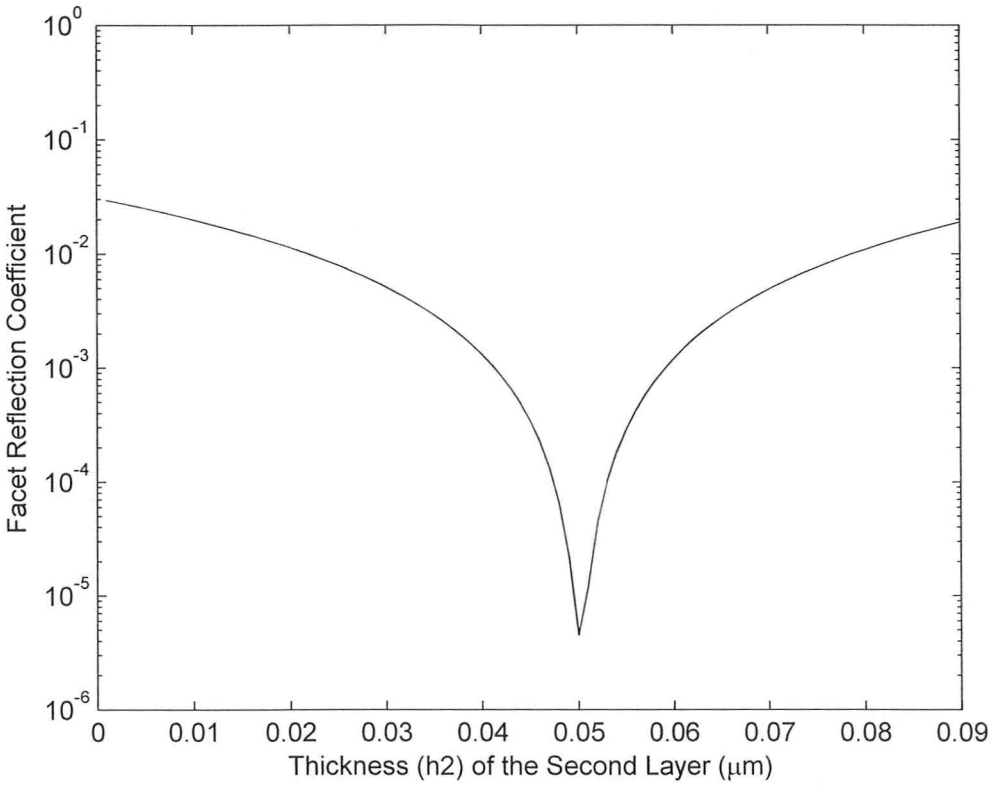

Fig. 8: Power reflection coefficient versus the second layer film thickness for a typical double-layer antireflection coated facet (TE). $n_1 = 3.524$, $n_2 = 3.17$, $n_3 = 1.82$, $n_4 = 1.65$, $d_1 = 0.11\,\mu m$, $d_2 = 3.6\,\mu m$, $d_3 = 0.5\,\mu m$, $h_1 = 0.1816\,\mu m$, and wavelength $\lambda = 1.54\,\mu m$.

Appendix B: Finite Difference (FD) Method for Mode Calculation

The modes for waveguide structures with arbitrary transverse index profiles have to be calculated by numerical methods. We will summarize the basic FD formulations below. An example for 2D mode calculation in a typical 3D waveguide structure is also given.

B.1 FD Scheme

Fig. 9 shows the positions of the nodes. The FD scheme for the governing equations involves the derivatives shown below. The PML regions can be similarly treated with the inclusion of the coordinate stretching factors.

$$\frac{\partial}{\partial x}\left[\frac{1}{n^2}\frac{\partial}{\partial x}(n^2 E_x)\right]_{(i,j)} = \frac{2}{h(i)(h(i)+h(i+1))}\cdot\frac{2n^2(i+1,j)}{n^2(i,j)+n^2(i+1,j)}\cdot E_x(i+1,j)$$

$$-\left[\frac{2}{h(i)(h(i)+h(i+1))}\cdot\frac{2n^2(i,j)}{n^2(i,j)+n^2(i+1,j)}+\frac{2}{h(i)(h(i)+h(i-1))}\cdot\frac{2n^2(i,j)}{n^2(i,j)+n^2(i-1,j)}\right]$$

$$\cdot E_x(i,j)+\frac{2}{h(i)(h(i)+h(i-1))}\cdot\frac{2n^2(i-1,j)}{n^2(i,j)+n^2(i-1,j)}\cdot E_x(i-1.j) \tag{2-59}$$

$$\left[\frac{\partial^2}{\partial y^2}(E_x)\right]_{(i,j)} = \frac{2}{h(j)(h(j)+h(j+1))}\cdot E_x(i,j+1)-\frac{2}{h(j)(h(j)+h(j+1))}\cdot E_x(i,j)$$

$$-\frac{2}{h(j)(h(j)+h(j-1))}\cdot E_x(i,j)+\frac{2}{h(j)(h(j)+h(j-1))}\cdot E_x(i,j-1) \tag{2-60}$$

$$\frac{\partial}{\partial x}\left[\frac{1}{n^2}\frac{\partial}{\partial y}(n^2 E_y)\right]_{(i,j)} = \frac{1}{\frac{h(i-1)}{2}+h(i)+\frac{h(i+1)}{2}}\cdot\frac{1}{\frac{h(j-1)}{2}+h(j)+\frac{h(j+1)}{2}}$$

$$\cdot\left[\frac{n^2(i+1,j+1)}{n^2(i+1,j)}\cdot E_y(i+1,j+1)-\frac{n^2(i+1,j-1)}{n^2(i+1,j)}\cdot E_y(i+1,j-1)\right. \tag{2-61}$$

$$\left.-\frac{n^2(i-1,j+1)}{n^2(i-1,j)}\cdot E_y(i-1,j+1)+\frac{n^2(i-1,j-1)}{n^2(i-1,j)}\cdot E_y(i-1,j-1)\right]$$

$$\frac{\partial}{\partial y}\left[\frac{\partial}{\partial x}(E_y)\right]_{(i,j)} = \frac{1}{\frac{h(i-1)}{2}+h(i)+\frac{h(i+1)}{2}} \cdot \frac{1}{\frac{h(j-1)}{2}+h(j)+\frac{h(j+1)}{2}} \tag{2-62}$$

$$\cdot\left[E_y(i+1,j+1)-E_y(i-1,j+1)-E_y(i+1,j-1)+E_y(i-1,j-1)\right]$$

$$\frac{\partial}{\partial y}\left[\frac{1}{n^2}\frac{\partial}{\partial y}(n^2 E_y)\right]_{(i,j)} = \frac{2}{h(j)(h(j)+h(j+1))} \cdot \frac{2n^2(i,j+1)}{n^2(i,j)+n^2(i,j+1)} \cdot E_y(i,j+1)$$

$$-\left[\frac{2}{h(j)(h(j)+h(j+1))} \cdot \frac{2n^2(i,j)}{n^2(i,j)+n^2(i,j+1)}\right.$$

$$\left.+\frac{2}{h(j)(h(j)+h(j-1))} \cdot \frac{2n^2(i,j)}{n^2(i,j)+n^2(i,j-1)}\right] \cdot E_y(i,j) \tag{2-63}$$

$$+\frac{2}{h(j)(h(j)+h(j-1))} \cdot \frac{2n^2(i,j-1)}{n^2(i,j)+n^2(i,j-1)} \cdot E_y(i,j-1)$$

$$\left[\frac{\partial^2}{\partial x^2}(E_y)\right]_{(i,j)} = \frac{2}{h(i)(h(i)+h(i+1))} \cdot E_y(i+1,j) - \frac{2}{h(i)(h(i)+h(i+1))} \cdot E_y(i,j)$$

$$-\frac{2}{h(i)(h(i)+h(i-1))} \cdot E_y(i,j) + \frac{2}{h(i)(h(i)+h(i-1))} \cdot E_y(i-1,j) \tag{2-64}$$

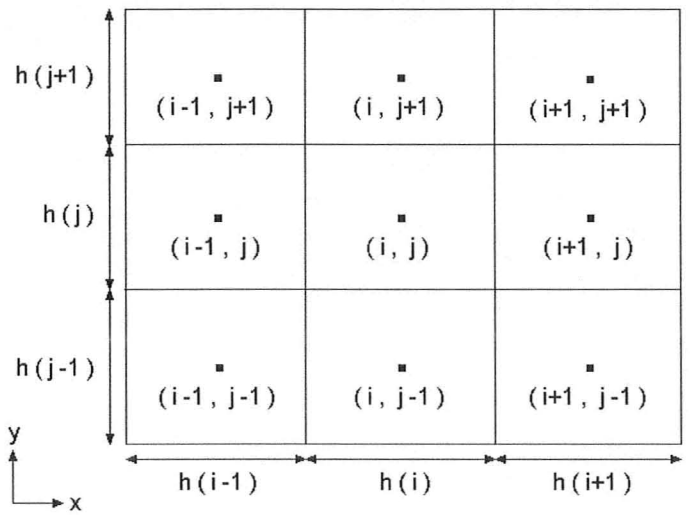

Fig. 9: Positions of the nodes for FD scheme. The node is located at the center of the cell and the medium in each cell is uniform.

$$\frac{\partial}{\partial y}\left[\frac{1}{n^2}\frac{\partial}{\partial x}(n^2 E_x)\right]_{(i,j)} = \frac{1}{\frac{h(i-1)}{2}+h(i)+\frac{h(i+1)}{2}} \cdot \frac{1}{\frac{h(j-1)}{2}+h(j)+\frac{h(j+1)}{2}}$$

$$\cdot\left[\frac{n^2(i+1,j+1)}{n^2(i,j+1)}\cdot E_x(i+1,j+1) - \frac{n^2(i-1,j+1)}{n^2(i,j+1)}\cdot E_x(i-1,j+1)\right. \tag{2-65}$$

$$\left. - \frac{n^2(i+1,j-1)}{n^2(i,j-1)}\cdot E_x(i+1,j-1) + \frac{n^2(i-1,j-1)}{n^2(i,j-1)}\cdot E_x(i-1,j-1)\right]$$

$$\frac{\partial}{\partial x}\left[\frac{\partial}{\partial y}(E_x)\right]_{(i,j)} = \frac{1}{\frac{h(i-1)}{2}+h(i)+\frac{h(i+1)}{2}} \cdot \frac{1}{\frac{h(j-1)}{2}+h(j)+\frac{h(j+1)}{2}} \tag{2-66}$$

$$\cdot\left[E_x(i+1,j+1) - E_x(i+1,j-1) - E_x(i-1,j+1) + E_x(i-1,j-1)\right]$$

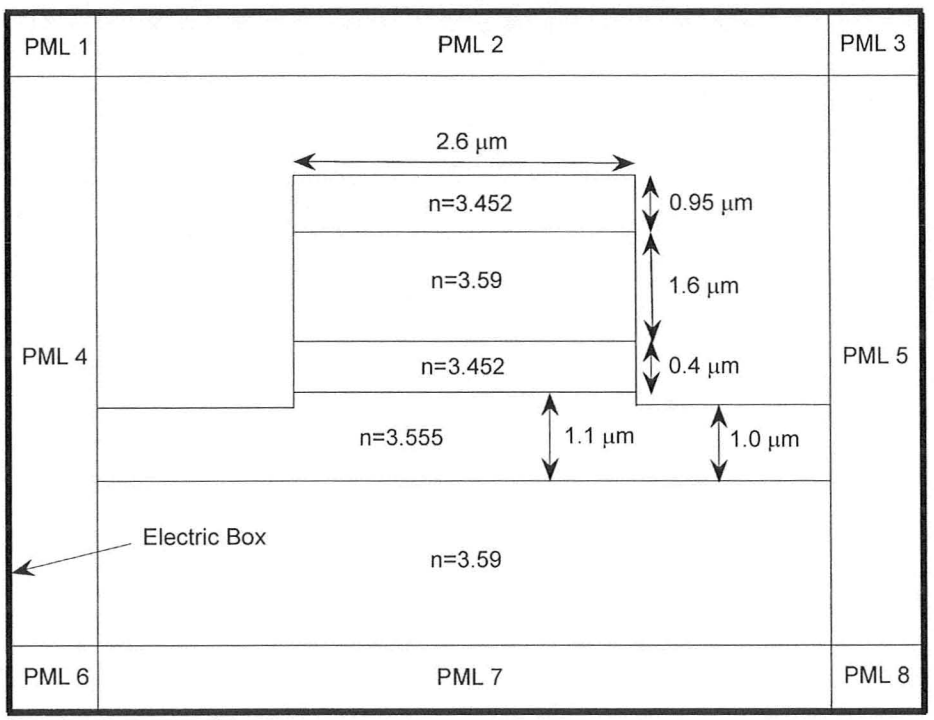

Fig. 10: A typical 3D leaky waveguide.

B.2 Application

We consider a typical 3D leaky waveguide [25] shown in Fig. 10. There are eight PML regions, and the coordinate stretching factors in each PML region are shown in Table I. We aim to calculate the symmetric quasi-TE modes (E_x modes) by using the semi-vectorial FD method. Only half of the whole structure needs to be considered due to the symmetry. As mentioned above, the nodes are all at the centers of the cells, and the medium is uniform in each cell. Note the nodes are also on the outside boundary and the symmetric line. The discretized semi-vectorial wave equation for the quasi-TE modes (E_x) at node (i, j) can be written as

$$B_1 E_x(i, j-1) + B_2 E_x(i-1, j) + B_3 E_x(i, j) + B_4 E_x(i+1, j) + B_5 E_x(i, j+1) = \beta^2 E_x(i, j) \tag{2-67}$$

where B_1, B_2, ..., and B_5 are the coefficients which can be obtained easily from FD formulations. Table II shows the computed normalized propagation constants of two symmetric quasi-TE modes by the semi-vectorial FD method. The results agree well with those by the finite element imaginary distance beam propagation method (FE-ID-BPM) [25]. The electric field distributions for these modes are shown in Fig. 11.

Table I: Coordinate stretching factors in the PML regions.

PML regions	Coordinate stretching factors	
PML (1)	s_x	s_y
PML (2)	1	s_y
PML (3)	s_x	s_y
PML (4)	s_x	1
PML (5)	s_x	1
PML (6)	s_x	s_y
PML (7)	1	s_y
PML (8)	s_x	s_y

Table II: Complex propagation constants of the symmetric quasi-TE modes. Wavelength $\lambda = 1.064\mu m$ and PML reflection coefficient $R = 10^{-8}$.

Modes	FD	FE-ID-BPM (Reference)
E_{11}^{x}	$3.573843 - j1.73384\times10^{-7}$	$3.574131 - j1.6976\times10^{-7}$
E_{12}^{x}	$3.543427 - j5.46652\times10^{-5}$	$3.543530 - j5.4823\times10^{-5}$

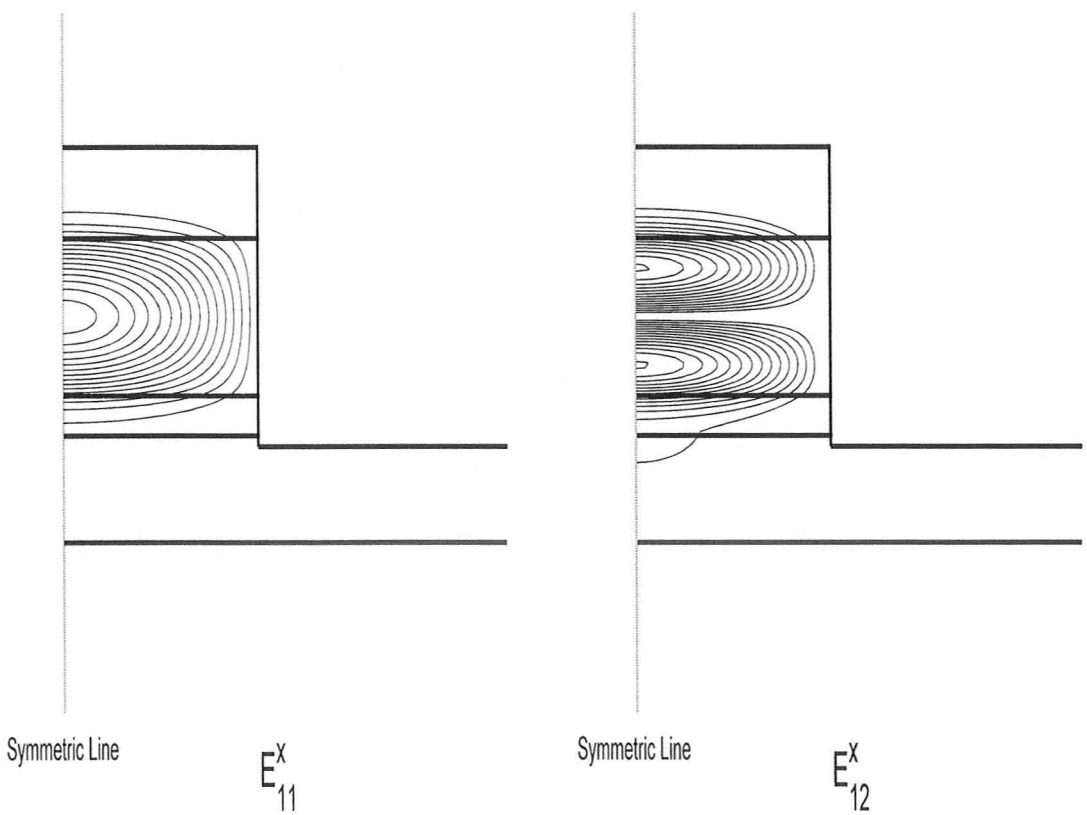

Fig. 11: Electric field distributions of two symmetric quasi-TE modes for a leaky waveguide.

Chapter 3

PML Effects on Mode Matching Solutions

The PML is introduced as a lateral absorbing medium in the closed waveguide structure so that the incident waves would not be reflected back to the non-PML medium. As stated, the box modes become complex. The effective indices and field patterns of these complex modes depend on the parameters of the PML such as PML thickness and attenuation in the PML. The complex modes are to be included in the modal expansion, and the mode matching solutions would be affected by the PML parameters. Such effects have to be investigated. We consider an open waveguide structure. It is surrounded by a perfectly conducting electric box where the tangential electric field component vanishes. The box can be seen as a lateral boundary which would reflects the incoming waves. For the waveguide with longitudinal discontinuities, the accuracy of the solution of the original problem depends on the size of the box and also the number of modes required for convergence. The farther away from the waveguide core the boundary is, the higher the achievable accuracy is, and consequently more number of modes is required in the modal expansion. The convergence rate is low. To obtain the reasonable results, we have to put the boundary sufficiently far away from the guiding region of the waveguide structure and therefore a large number of box modes are needed. A typical example [26] is the step discontinuity of the planar dielectric waveguide shown in Fig. 12. It can be demonstrated that the reflection coefficients in the waveguide structure enclosed by the perfectly conducting electric walls (without the PML) oscillate with respect to the

distance from the boundary (electric wall) to the center of the waveguide. The magnitude of such oscillation is related to the excitation of the box modes. Obviously, the solutions suffer from convergence difficulties.

When the absorbing PML is introduced, we can treat the waveguide structure as if it is an open one. With the properly chosen PML parameters, the complex modes can be used in the modal expansion instead of radiation or leaky modes. The coordinate-stretching factors s_x and s_y in (2-18a) and (2-18b) are used to describe the properties of the PML. The parameter σ (σ_x or σ_y) controls the decay of the propagating waves in the PML region; the real part κ (κ_x or κ_y) causes additional attenuation of the evanescent waves. It indicates that the PML can absorb both propagating and evanescent waves effectively [27]. Since the box is located where the amplitudes of the fields of the guided waves are sufficiently small, for instance, lower than a prescribed value, the real parts κ_x and κ_y of the coordinate-stretching factors can be set 1.

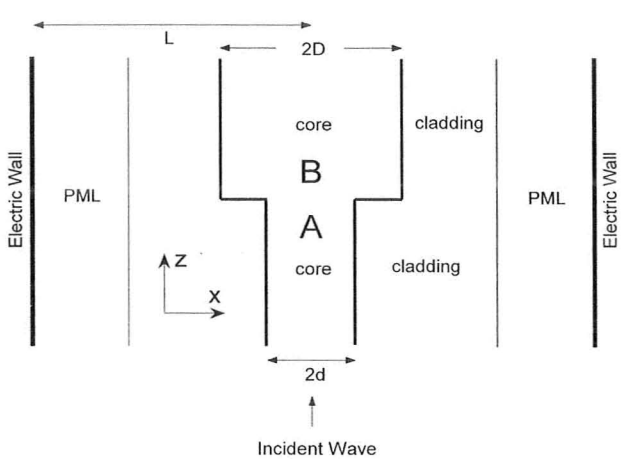

Fig. 12: Step discontinuity of a planar dielectric waveguide surrounded by the perfectly conducting electric walls with the inner PML. The whole structure is symmetric. L is the distance from the electric wall to the center.

Now we consider the imaginary parts of the coordinate-stretching factors. The parameter σ (σ_x or σ_y) usually takes the following form [7]

$$\sigma = \sigma_{\max}(\frac{\rho}{d_{PML}})^m, \qquad m = 1, 2, 3, ... \tag{3-1}$$

where d_{PML} is the PML thickness and ρ is the distance from the start point of the PML. There may be other spatial profiles of σ. It is expected that the solutions would not be affected significantly by the forms of the parameter σ. We have chosen the profile to be parabolic, i.e., $m = 2$, which has been commonly used in FDTD simulation. For convenience, we can define a PML reflection coefficient from which the maximum value $\sigma_{\max}$ in (3-1) can be calculated.

We assume a plane wave perpendicularly incident into the PML region (see Fig. 13). The electric field for the plane wave is given by

$$E = E_0 \exp(-jk\tilde{x}) \tag{3-2}$$

where $k = \frac{\omega n}{c}$, n is the index of refraction in the non-PML and PML regions, and c is the speed of light in free space. The coordinate-stretching factor s in the PML region is $1 - j\frac{\sigma}{\omega\varepsilon_0 n^2}$. We can easily obtain the PML reflection coefficient R at the interface between the non-PML and PML regions

$$R = \exp\left[-\frac{2\sigma_{\max}}{c\varepsilon_0 n}\int_0^{d_{PML}}(\frac{\rho}{d_{PML}})^m d\rho\right]. \tag{3-3}$$

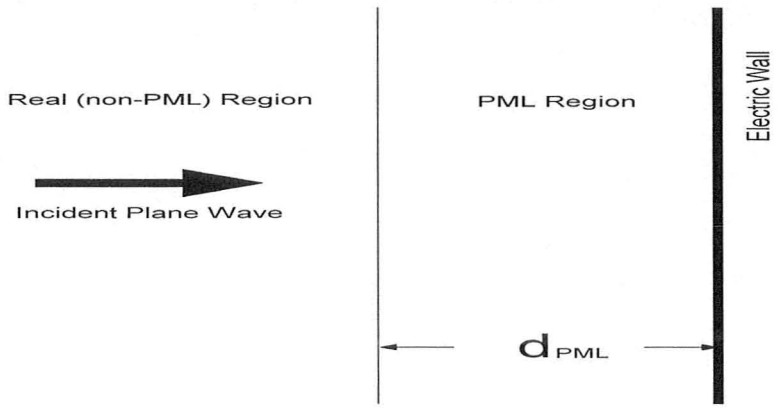

Fig. 13: A plane wave perpendicularly incident into the PML region.

Therefore, we can write the coordinate stretching factor as follows

$$s(\rho) = 1 - j\frac{\sigma}{\omega\varepsilon_0 n^2} = 1 - j\frac{\lambda}{4\pi n d_{PML}}\left[(m+1)\ln\frac{1}{R}\right](\frac{\rho}{d_{PML}})^m . \qquad (3\text{-}4)$$

Since the PML is introduced as an absorbing medium to reduce the unwanted reflection to the guiding region of the waveguide structure in the MMM, the PML reflection coefficient R representing the attenuation level within the PML plays a key role in the choice of the PML parameters. It can be seen from (3-3) that the PML reflection coefficient R reflects the collective effects of all PML parameters such as $\sigma_{\max}$ and PML thickness. The smaller the PML reflection coefficient is, the more effective the PML is. In practice, the value of the PML reflection coefficient must be lower than certain level to ensure the sufficient accuracy of the mode matching calculation, as demonstrated below. We have investigated some of these combinations such as $\sigma_{\max}$ and d_{PML} and found that they make negligible impact on the accuracy of the mode matching calculation for the same value of the PML reflection coefficient. As an example, we compute the

dependence of the amplitude of the reflection coefficient (TE) for incidence from waveguide A on the PML thickness in the planar step discontinuity when the PML reflection coefficient R is 0.01. The results are shown in Fig. 14. It can be seen that PML thickness doesn't have significant effects on the solutions. Although the PML thickness can be chosen arbitrarily as long as the guided waves in the waveguide are not affected, it should not be too small, otherwise the values of the parameters σ_x and σ_y must be large enough in order to keep the PML reflection coefficient small, i.e., the PML still effective, in the mode matching calculation. The sharp variation of the parameters σ_x and σ_y within the PML region is not preferred in the numerical computation.

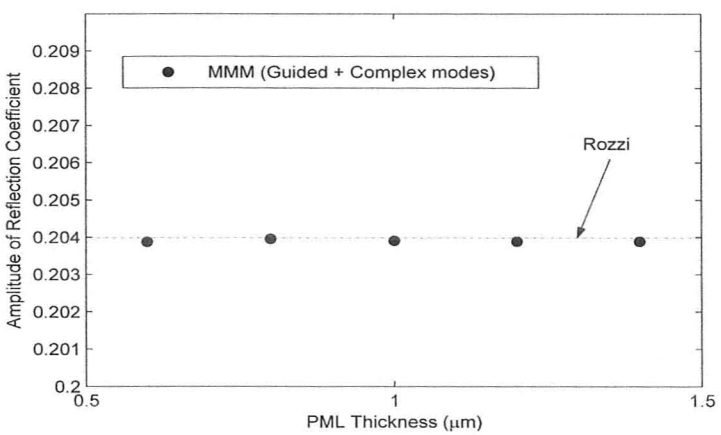

Fig. 14: Amplitude of reflection coefficient for incidence from waveguide A versus PML thickness for the planar step discontinuity (TE). $n_{core} = 2.236$, $n_{cladding} = 1.0$, $D = 0.2387\mu m$, $d = 0.2D$, $L = 3.2387\mu m$, and wavelength $\lambda = 1.5\mu m$.

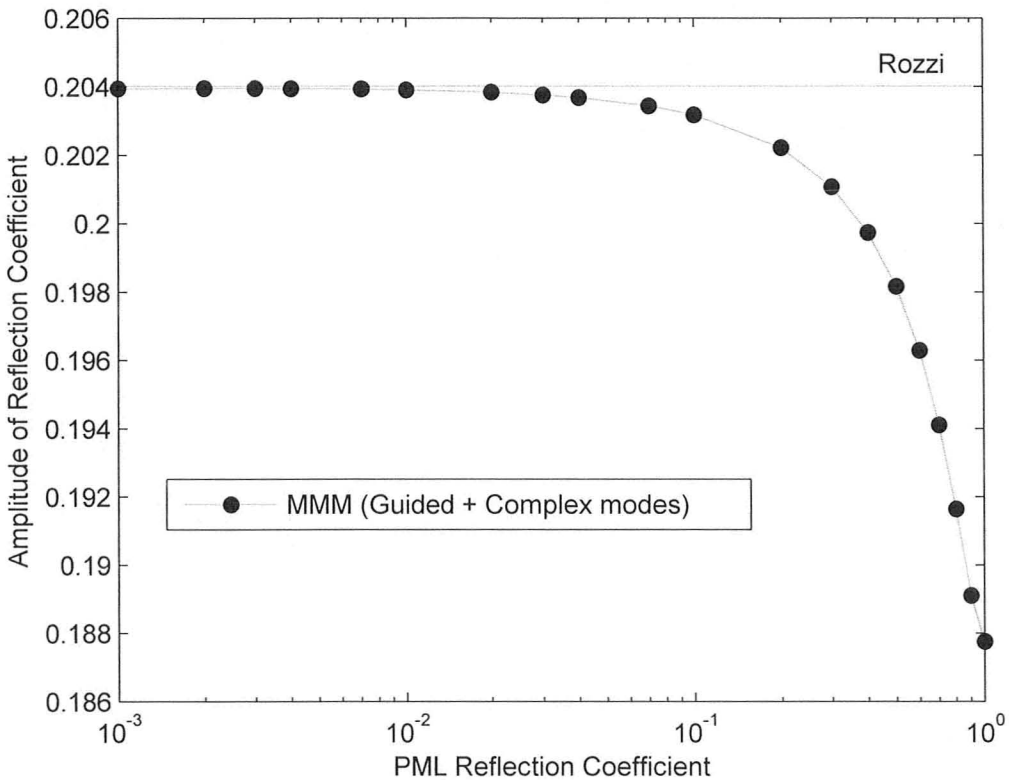

Fig. 15: Amplitude of reflection coefficient for incidence from waveguide A versus the PML reflection coefficient R for the planar step discontinuity (TE). $n_{core} = 2.236$, $n_{cladding} = 1.0$, $D = 0.2387\mu m$, $d = 0.2D$, $L = 3.2387\mu m$, and wavelength $\lambda = 1.5\mu m$.

As we mentioned above, without the presence of the PML the convergence is difficult due to the oscillation of the solutions with respect to the position of the electric wall in the example. While the PML is introduced to reduce the unwanted reflection, the amplitude of the oscillation is reduced accordingly. We may set a small value for the amplitude. When the amplitude is smaller than the prescribed value, the corresponding R is selected, and the mode matching solution is acceptable. We have calculated the amplitudes of the reflection coefficients (TE) for incidence from waveguide A for the

different values of the PML reflection coefficient R in the planar step discontinuity. The computed results are shown in Fig. 15, and that by Rozzi is also shown for comparison. It can be seen that a good agreement is achieved when $R \leq 0.01$. There are no significant improvements when R is reduced further. The comparison with Rozzi's results (the reflection coefficient and loss) is also shown in Table III.

It is expected that for a PML with strong attenuation, the mode spectrum can be clearly divided into three groups [8] [28] [29]. The first group includes guided modes with modal effective indices on the real axis in the complex plane. These guided modes are not disturbed significantly by the introduction of the PML. The modes in the second group are called quasi-leaky modes whose field distributions grow exponentially into the cladding and get dumped in the PML region. The modes in the third group are PML modes. The field of the PML mode is mainly concentrated in the PML region, and hence the PML mode is more orthogonal to the incident fundamental guided mode which has substantial field in the core and to some extent cladding region close to the waveguide core. Consequently, the contribution of the PML modes in the modal expansion is smaller.

Table III: Comparison between the MMM and Rozzi's method for the planar step discontinuity (TE). PML reflection coefficient is 0.01. r_1 is the amplitude of reflection coefficient for incidence from waveguide A. The loss refers to incidence from waveguide A.

	$\lvert r_1 \rvert$	$\angle r_1 - \pi$	Loss
MMM	0.2039	-0.0861	0.0719
Rozzi	0.2040	-0.0860	0.0718

Chapter 4

Application to 3D Waveguide Structures

We have investigated the effects of the PML parameters on the mode matching solutions. In this Chapter, we will apply the complex MMM for analysis of practical 3D waveguide structures with longitudinal discontinuities. Semi and full-vectorial FD methods are used for 2D mode calculation. As discussed, we assume for all the simulation that the whole waveguide structure is enclosed by a perfectly conducting box with the inner PML. The new introduced boundary is located where the amplitudes of the guided waves are sufficiently small. Beyond this point, the position of the boundary becomes less important and would not affect the solutions significantly when the PML is strong enough. It indicates that the box with the inner PML may be located closer to the waveguide core than the box without the PML, and hence the computation effort would be greatly reduced for mode calculation and the MMM. In the following, we will first assess the semi-vectorial method via an example, and then apply the semi-vectorial FD method and mode matching technique for analysis of waveguide air gap and facet. Finally, the properties of the polarization converter are computed by the full-vectorial method.

4.1 Assessment of the Semi-Vectorial Method

In the semi-vectorial method for analysis of the 3D waveguide structures, the polarization coupled terms are simply ignored, and the resultant wave equations are greatly simplified. In practice, the semi-vectorial wave equations can be used to analyze

many optical devices in which these coupling terms can be neglected. It was demonstrated that the semi-vectorial method can yield sufficiently accurate results with much less computation time. We consider a rectangular dielectric waveguide, and calculate the propagation constants and the field patterns by solving the modal governing equations with and without the polarization coupled terms. We also check the orthogonality relations of the semi-vectorial modes. The waveguide core width is $1.0\mu m$, and its thickness is $0.5\mu m$. The indices of refraction of the core and the cladding are 3.44 and 3.39, respectively. The wavelength λ is $0.86\mu m$. The PML reflection coefficient R is set 10^{-7}. It is a waveguide structure with low index contrast. It is shown that the errors of the solutions by the full-vectorial and semi-vectorial methods are less than 1.5×10^{-4} for both normalized propagation constants (real or imaginary parts) and the field patterns of the major components of the first four computed quasi-TE modes. The errors for the orthogonality relationship of the normalized semi-vectorial modes are found to be lower than 10^{-5} for the first four quasi-TE modes. Note that we have employed the following criterion to evaluate the orthogonality relations of the computed semi-vectorial modes

$$Error = \sum_{\substack{n=1 \\ (n\neq m)}}^{N} \left| < \vec{e}_{tm}, \vec{h}_{tn} > \right| = \sum_{\substack{n=1 \\ (n\neq m)}}^{N} \left| \frac{1}{2} \iint_S (\vec{e}_{tm} \times \vec{h}_{tn}) \cdot \hat{z}\, ds \right| < \varepsilon \qquad (4\text{-}1)$$

where N is the number of modes to be considered, and ε is a prescribed value. From the computed results, we see that the semi-vectorial method is very effective for mode calculation, and the semi-vectorial modes can be used in the modal expansion in the MMM. The common orthogonality relationship can also be utilized since the non-

orthogonality error between the normalized semi-vectorial modes is negligibly small as demonstrated above. It has to be mentioned that the semi-vectorial approximation may be subject to considerable errors if the polarization coupling between two semi-vectorial modes in a waveguide structure can not be ignored. Under this circumstance, the MMM based on semi-vectorial modal expansion is no longer valid, and the rigorous full-vectorial method must be used.

4.2 Application

4.2.1 Waveguide Air Gap

The waveguide air gap is often encountered in integrated optics. It is important to analyze its reflection, transmission and loss properties. We consider two equal dielectric rectangular waveguides with air gap shown in Fig. 16 [30]. Waveguide core width is $L_x = 1.0\mu m$, and core thickness is $L_y = 0.5\mu m$. The indices of refraction of core and cladding are 3.44 and 3.39, respectively. The wavelength λ is $0.86\mu m$. The waveguide core is located at the center of the computation domain. The cross-section for the waveguide structure is shown in Fig. 17. The entire PML medium is divided into eight regions. For each region, the coordinate stretching factors are set according to Table I. We set the PML reflection coefficient $R = 0.01$. The power reflection, transmission, and loss coefficients for an incident guided wave (quasi-TE) are calculated. There are three waveguide sections along the longitudinal direction. The S matrix cascade is used to connect the fields of the different waveguide sections. We set $D_x = 3.0\mu m$ and $D_y = 2.0\mu m$. Fig. 18, Fig. 19 and Fig. 20 show the computed power reflection,

transmission and loss coefficients by the MMM, respectively. 90 modes are used in the modal expansion. It is expected that the larger box size does not have significant effects on the mode matching solutions due to the introduction of the PML with properly chosen parameters. We also checked the number of modes used for the mode matching calculation. Fig. 21 shows the effects of the number of modes on the power transmission coefficients. It is found that good results can be obtained when the number of modes are larger than 60.

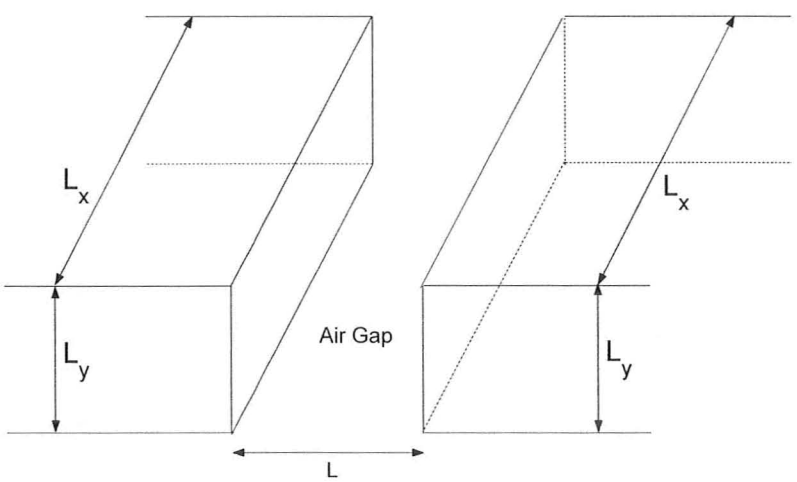

Fig. 16: Waveguide air gap.

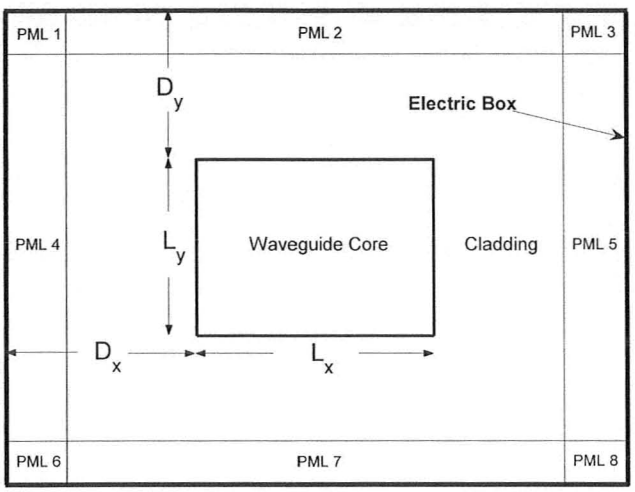

Fig. 17: The cross-section for a rectangular dielectric waveguide enclosed by a perfectly conducting electric box with the inner PML. The waveguide core is located at the center of the whole structure.

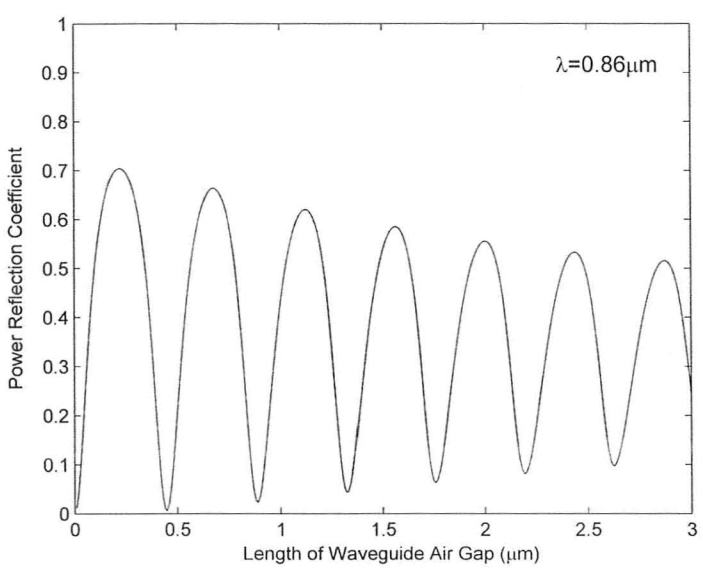

Fig. 18: Power reflection coefficient versus the length of the waveguide air gap (quasi-TE). $D_x = 3.0\mu m$, $D_y = 2.0\mu m$, $L_x = 1.0\mu m$, $L_y = 0.5\mu m$, $n_{core} = 3.44$, $n_{cladding} = 3.39$, and wavelength $\lambda = 0.86\mu m$.

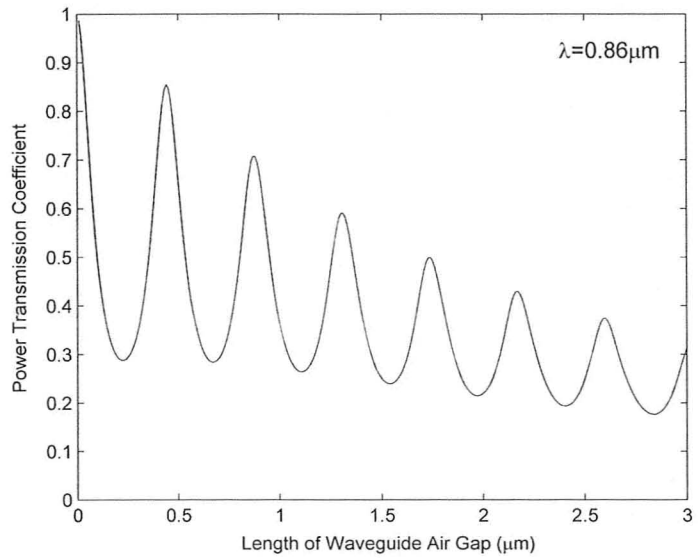

Fig. 19: Power transmission coefficient versus the length of the waveguide air gap (quasi-TE). $D_x = 3.0\mu m$, $D_y = 2.0\mu m$, $L_x = 1.0\mu m$, $L_y = 0.5\mu m$, $n_{core} = 3.44$, $n_{cladding} = 3.39$, and wavelength $\lambda = 0.86\mu m$.

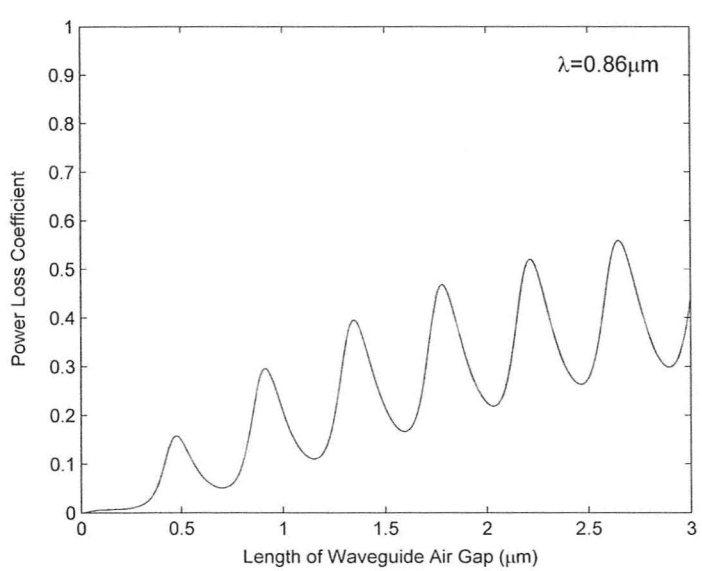

Fig. 20: Power loss coefficient versus the length of the waveguide air gap (quasi-TE). $D_x = 3.0\mu m$, $D_y = 2.0\mu m$, $L_x = 1.0\mu m$, $L_y = 0.5\mu m$, $n_{core} = 3.44$, $n_{cladding} = 3.39$, and wavelength $\lambda = 0.86\mu m$.

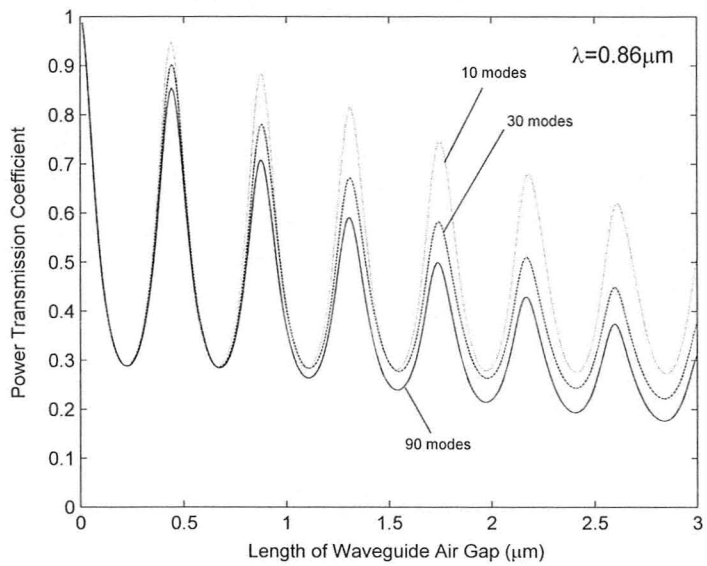

Fig. 21: Power transmission coefficients versus the length of the waveguide air gap for different number of modes (quasi-TE). $D_x = 3.0\mu m$, $D_y = 2.0\mu m$, $L_x = 1.0\mu m$, $L_y = 0.5\mu m$, $n_{core} = 3.44$, $n_{cladding} = 3.39$, and wavelength $\lambda = 0.86\mu m$.

4.2.2 Waveguide Facet

In this section, we calculate the reflection coefficient of a rectangular waveguide facet [31]. The waveguide width is L_x, and the thickness is $L_y = 0.5L_x$. The wavelength is $\lambda = 0.86\mu m$. We define a normalized core thickness as follows

$$h = \frac{2L_y\sqrt{n_{core}^2 - n_{cladding}^2}}{\lambda} \tag{4-2}$$

where n_{core} and $n_{cladding}$ are the indices of refraction of waveguide core and cladding, respectively. Fig. 22 shows the computed power reflection coefficient (quasi-TE) versus the normalized core thickness. The results agree well with those in the literature.

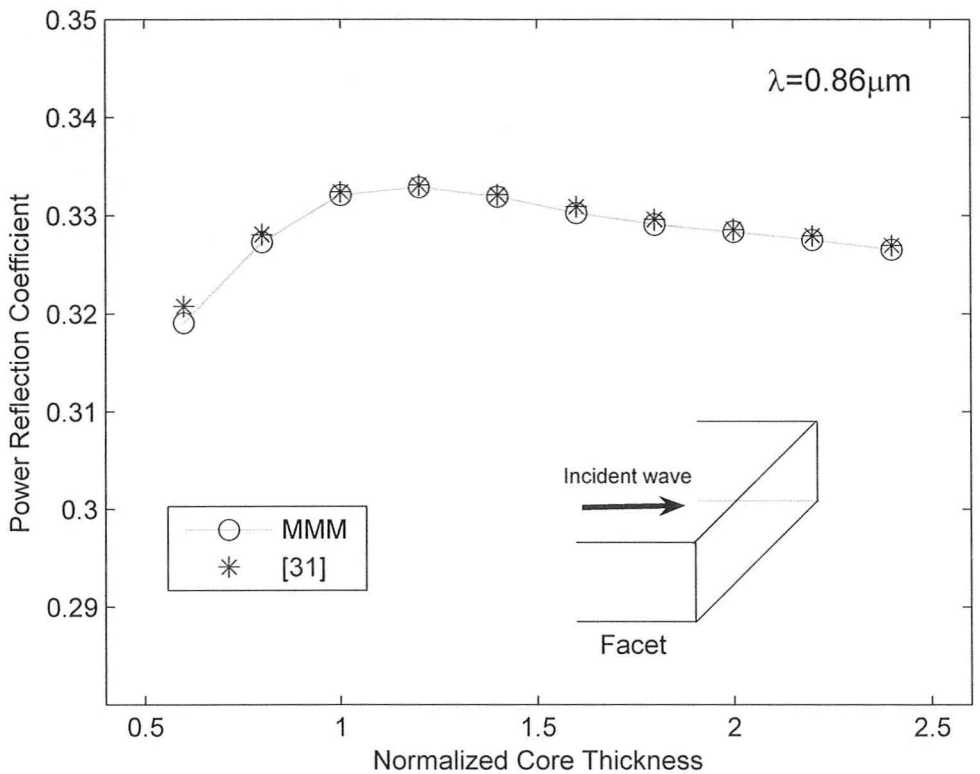

Fig. 22: Power reflection coefficient versus normalized core thickness for the waveguide facet (quasi-TE). $n_{core} = 3.6$, $n_{cladding} = 3.492$, $L_y = 0.5L_x$, and wavelength $\lambda = 0.86\mu m$.

4.2.3 Polarization Converter

The polarization converter has been used in many applications such as polarization diversity receivers in coherent optical communications. Since a new passive polarization converter made of asymmetric periodic loaded rib waveguides was proposed [32], a variety of methods have been utilized to explain the principle of operation and evaluate the polarization conversion properties. The coupled mode theory based on scalar modes first gave a theoretical analysis of the passive polarization converter [33]. A

physical picture for the operation principle was presented by way of the normal mode analysis. On the other hand, the full-vectorial beam propagation method (FV-BPM) was also utilized [34] [35] for computing the characteristics of polarization converters and has been proved to be very effective.

The scalar and semi-vectorial methods are inadequate for the analysis of polarization rotation unless vector correction is applied. Although the polarization dependence is considered in the semi-vectorial method, the polarization coupling is ignored. For accurate analysis, the full-vectorial method has to be used for investigating the polarization conversion properties. Here we use the MMM to calculate the polarization conversion properties of an asymmetric periodic loaded rectangular waveguide [35]. The full-vectorial FD method is utilized. The reflected waves are included in the modal expansion. Radiation waves are represented by discrete complex modes.

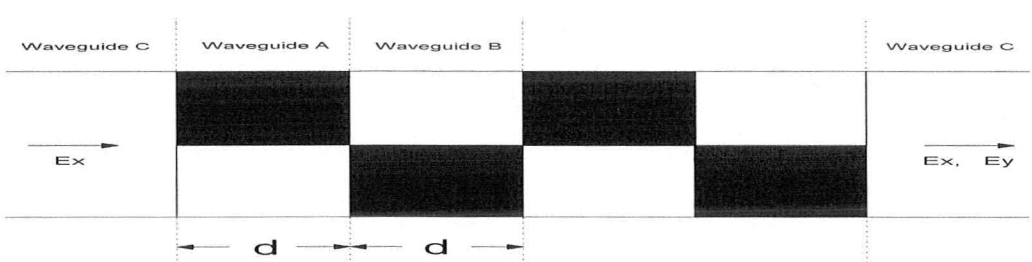

Fig. 23: Top view of an asymmetric loaded rectangular waveguide.

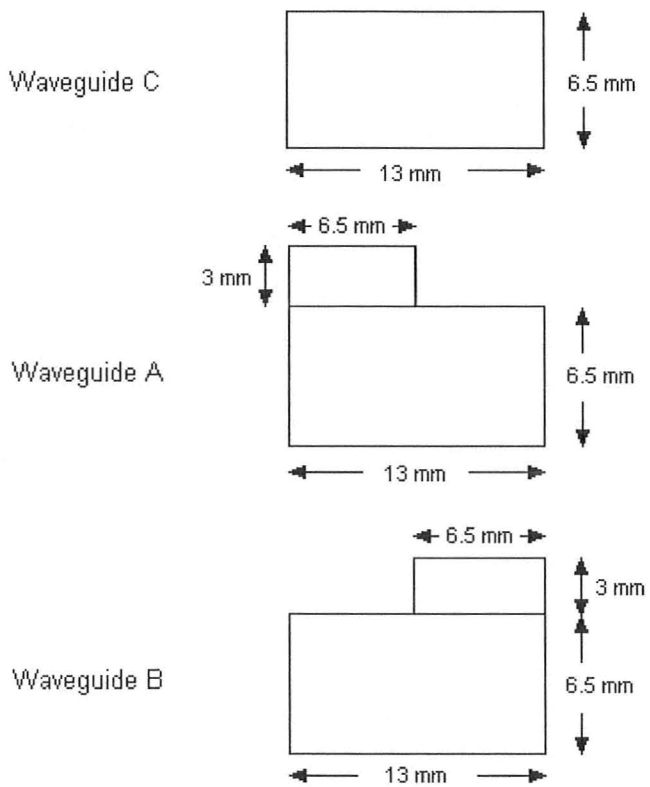

Fig. 24: Cross-section of an asymmetric loaded rectangular waveguide.

The top view and cross-section configurations of the asymmetric loaded rectangular waveguide are shown in Fig. 23 and Fig. 24. The width and thickness of the rectangular waveguide are 13mm and 6.5mm, respectively. The width of the load is 6.5mm; the thickness is 3mm. The relative permittivity of the rectangular waveguide and load is 2.8. The operating wavelength is 20mm. The length of the load is given by

$$d = \frac{\pi}{\beta_{Ex} - \beta_{Ey}} \tag{4-3}$$

where β_{Ex} and β_{Ey} are the propagation constants of dominant E^x and E^y modes in the loaded waveguide, respectively. The propagation constants can be obtained by the full-

vectorial FD method. It is found that the value of d for the waveguide structure is 160mm. The electric field distributions for the waveguide structures are shown in Fig. 25, Fig. 26, and Fig. 27. An incoming guided wave, called E_{11}^{x} mode, is launched from section C into the loading region. The dependence of the mode power on the number of loads is calculated. Fig. 28 shows the computed power conversion properties. We can see that the conversion can be achieved after three loads.

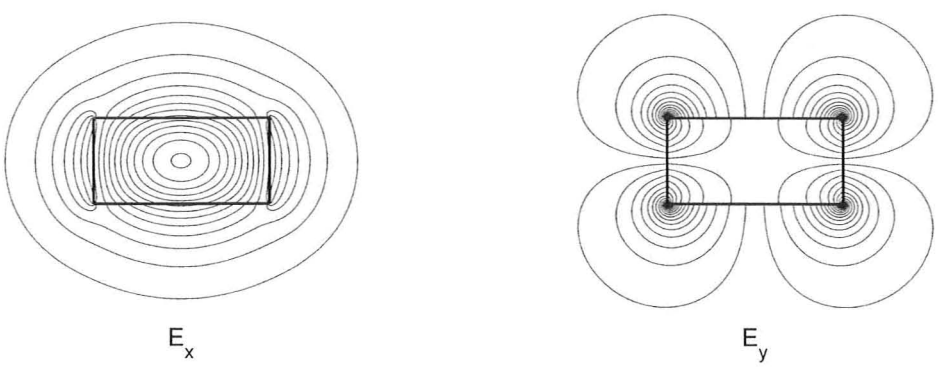

Fig. 25: Electric field distributions of the fundamental quasi-TE mode for waveguide C (without loads).

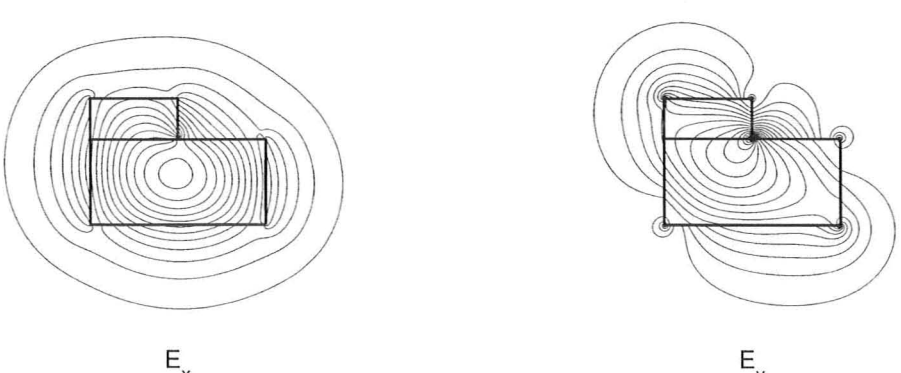

Fig. 26: Electric field distributions of the fundamental quasi-TE mode for waveguide A in the asymmetric loaded rectangular waveguide.

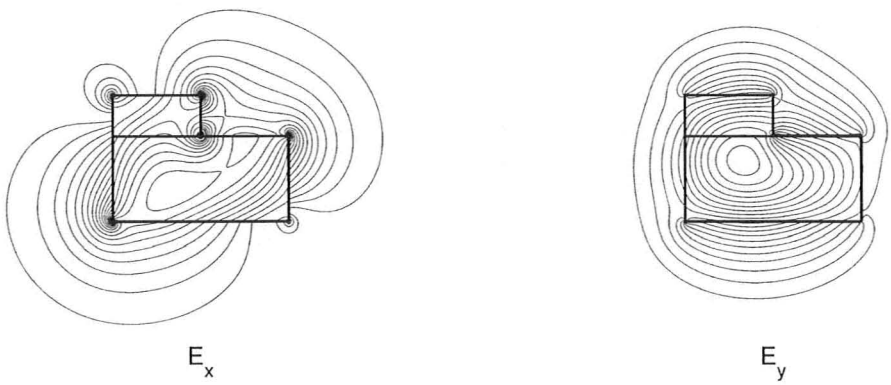

Fig. 27: Electric field distributions of the fundamental quasi-TM mode for waveguide *A* in the asymmetric loaded rectangular waveguide.

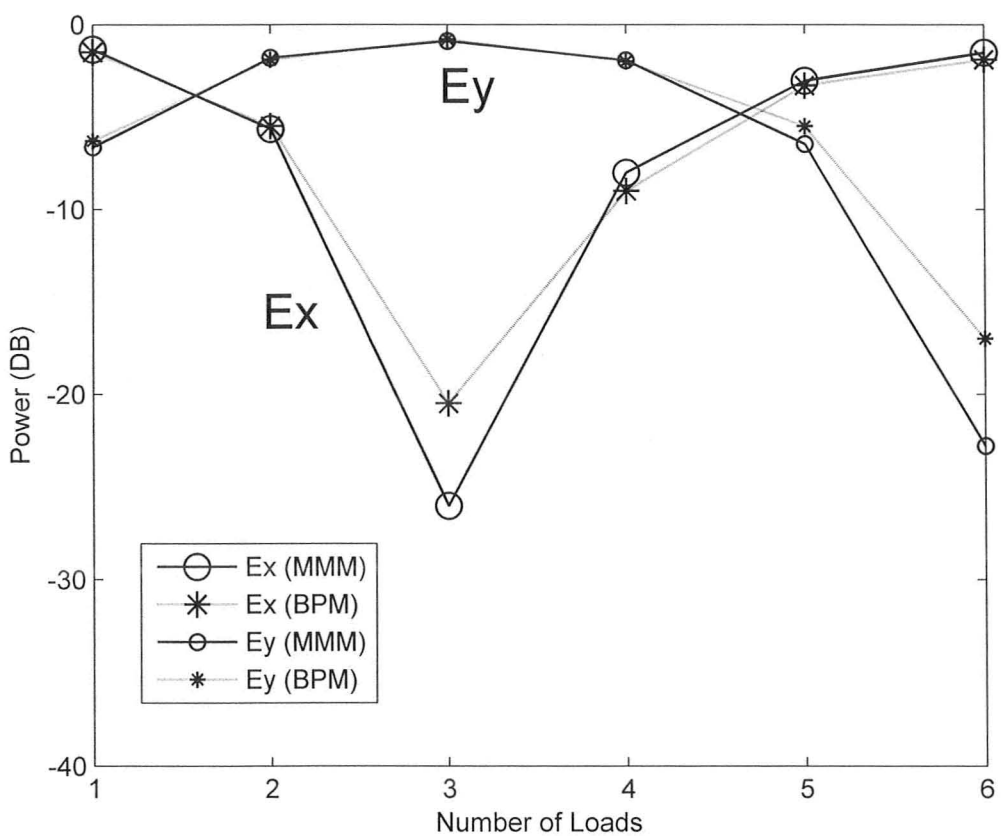

Fig. 28: Mode power (DB) versus number of loads for the asymmetric loaded rectangular waveguide.

Chapter 5

Conclusions

The conventional mode matching technique has been extended to deal with the problems of 3D open dielectric waveguide structures with arbitrary index profiles and longitudinal discontinuities. The perfectly conducting box with the inner PML was introduced as a lateral boundary to absorb the incoming waves so that the discrete complex modes were formed. These complex modes dependent on the PML parameters were used in the modal expansion to represent the radiation or leaky modes of the original open waveguide structure. It was shown that the representation in terms of the guided and complex modes in the MMM is more effective and the difficulties arising from the inclusion of the continuous radiation modes can be avoided.

Several examples were analyzed in order to demonstrate the application of the method. For waveguide air gap and facet, the semi-vectorial modes were used to expand the fields. The numerical results for the facet were compared with those in the literature. Good agreement was achieved over a wide range of the waveguide parameter. The conversion properties for an asymmetric loaded waveguide polarization converter were calculated by the full-vectorial MMM since the polarization coupling must be considered. The results were in good agreememt with those by BPM. The effectiveness was verified.

The effects of the PML parameters on the mode matching solutions were also investigated. The discussion focused on the PML reflection coefficient R. It was shown that the PML reflection coefficient R is a key parameter in the complex MMM and needs

to be chosen properly. We also demonstrated that the PML thickness has no significant effects on the solutions if R is the same.

Bibliography

[1] G. V. Eleftheriades, A. S. Omar, L. P. B. Katehi, and G. M. Rebeiz, "Some important properties of waveguide junction generalized scattering matrices in the context of the mode matching technique," *IEEE Trans. Microwave Theory Tech.*, vol. 42, pp. 1896-1903, Oct. 1994.

[2] K. L. Chan and S. R. Judah, "Mode-matching analysis of a waveguide junction formed by a circular and a larger elliptic waveguide," *IEE Proc. Microw. Antennas Propag.*, vol. 145, pp. 123-127, Feb. 1998

[3] S. L. Lin, L. W. Li, T. S. Yeo, and M. S. Leong, "Novel unified mode matching analysis of concentric waveguide junctions," *IEE Proc. Microw. Antennas Propag.*, vol. 148, pp. 369-374, Dec. 2001.

[4] A. W. Snyder and J. D. Love, *Optical Waveguide Theory*. London: Chapman and Hall, 1983.

[5] D. Marcuse, *Theory of Dielectric Optical Waveguides*, Second Edition, 1991.

[6] R. Sammut and A. W. Snyder, "Leaky modes on a dielectric waveguide: orthogonality and excitation," *Appl. Opt.*, vol. 15, pp. 1040-1044, Apr. 1976.

[7] J. P. Berenger, "A perfectly matched layer for the absorption of electromagnetic waves," *J. Comput. Phys.*, vol. 114, pp. 185-200, 1994.

[8] H. Derudder, F. Olyslager, D. De Zutter, and S. Van den Berghe, "Efficient mode-matching analysis of discontinuities in finite planar substrates using perfectly matched layers," *IEEE Trans. Antennas Propagat.*, vol. 49, pp. 185-195, Feb. 2001.

[9] H. Derudder, D. De Zutter, and F. Olyslager, "Analysis of waveguide discontinuities using perfectly matched layers," *Electron. Lett.*, vol. 34, pp. 2138-2140, Oct. 1998.

[10] P. Bienstman, H. Derudder, R. Baets, F. Olyslager, and D. De Zutter, "Analysis of cylindrical waveguide discontinuities using vectorial eigenmodes and perfectly matched layers," *IEEE Trans. Microwave Theory Tech.*, vol. 49, pp. 349-354, Feb. 2001.

[11] W. P. Huang (Editor), *Methods for Modeling and Simulation of Guided-Wave Optoelectronic Devices: Part I: Modes and Couplings, Progress in Electromagnetics Research* (Chief Editor: J. A. Kong), *Electromagnetic Waves*, PIER 10, 1995.

[12] M. S. Stern, "Semivectorial polarized finite difference method for optical waveguides with arbitrary index profiles," *IEE Proc. J*, 135, pp. 56-63, 1988.

[13] W. P. Huang and C. L. Xu, "Simulation of three-dimensional optical waveguides by a full-vector beam propagation method," *IEEE J. Quantum Electron.*, vol. 29, pp. 2639-2649, Oct. 1993.

[14] L. Vincetti, A. Cucinotta, S. Selleri, and M. Zoboli, "Three-dimensional finite-element beam propagation method: assessments and developments," *J. Opt. Soc. Am. A*, vol. 17, pp. 1124-1131, June 2000.

[15] C. A. De Francisco, B. V. Borges, and M. A. Romero, "A semivectorial method for the modeling of photonic crystal fibers," *Microwave Opt. Technol. Lett.*, vol. 38, no. 5, pp. 418-421, Sept. 2003

[16] P. Yeh, *Optical Waves in Layered Media*, 1988.

[17] W. C. Chew, J. M. Jin, and E. Michielssen, "Complex coordinate stretching as a generalized absorbing boundary condition," *Microwave Opt. Technol. Lett.*, vol. 15, no. 6, pp. 363-369, Aug. 1997.

[18] L. M. Delves and J. N. Lyness, " A numerical method for locating the zeros of an analytical function," *Math. Comp.*, vol. 21, pp. 543-560, 1967.

[19] R. E. Smith, S. N. Houde-Walter, and G. W. Forbes, "Mode determination for planar waveguides using the four-sheeted dispersion relation," *IEEE J. Quantum Electron.*, vol. 28, pp. 1520-1526, Jun. 1992.

[20] E. Anemogiannis and E. N. Glytsis, "Multilayer waveguides: efficient numerical analysis of general structures," *J. Lightwave Technol.*, vol. 10, pp. 1344-1351, Oct. 1992.

[21] S. D. Gedney, "An anisotropic perfectly matched layer-absorbing medium for the truncation of FDTD lattices," *IEEE Trans. Antennas Propagat.*, vol. 44, pp. 1630-1639, Dec. 1996.

[22] L. Li, "Multilayer modal method for diffraction gratings of arbitrary profile, depth, and permittivity," *J. Opt. Soc. Am. A,* vol. 10, pp. 2581-2591, Dec. 1993.

[23] L. Li, "Formulation and comparison of two recursive matrix algorithms for modeling layered diffraction gratings," *J. Opt. Soc. Am. A*, vol. 13, pp. 1024-1035, May. 1996.

[24] T. Saitoh, T. Mukai, and O. Mikami, "Theoretical analysis and fabrication of antireflection coatings on laser-diode facets," *J. Lightwave Technol.*, vol. 3, pp. 288-293, Apr. 1985.

[25] Y. Tsuji and M. Koshiba, "Guided-mode and leaky-mode analysis by imaginary distance beam propagation method based on finite element scheme," *J. Lightwave Technol.*, vol. 18, pp. 618-623, Apr. 2000.

[26] T. E. Rozzi, "Rigorous analysis of the step discontinuity in a planar dielectric waveguide," *IEEE Trans. Microwave Theory Tech.*, vol. 26, pp. 738-746, Oct. 1978.

[27] J. Fang, and Z. Wu, "Generalized perfectly matched layer for the absorption of propagating and evanescent waves in lossless and lossy media," *IEEE Trans. Microwave Theory Tech.*, vol. 44, pp. 2216-2222, Dec. 1996.

[28] H. Rogier and D. De Zutter, "Berenger and leaky modes in microstrip substrates terminated by a perfectly matched layer," *IEEE Trans. Microwave Theory Tech.*, vol. 49, pp. 712-715, Apr. 2001.

[29] H. Rogier and D. De Zutter, "Berenger and leaky modes in optical fibers terminated with a perfectly matched layer," *J. Lightwave Technol.*, vol. 20, pp. 1141-1148, July 2002.

[30] M. Reed, P. Sewell, T. M. Benson, and P. C. Kendall, "Efficient propagation algorithm for 3D optical waveguides," *IEE Proc. Optoelectron.*, vol. 145, pp. 53-58, Feb. 1998.

[31] A. Vukovic, P. Sewell, T. M. Benson, and P. C. Kendall, "Advances in facet design for buried lasers and amplifiers," *IEEE J. Quantum Electron.*, vol. 6, pp.175-184, Jan./Feb. 2000.

[32] Y. Shani, R. Alferness, T. Koch, U. Koren, M. Oron, B. I. Miller, and M. G. Young, "Polarization rotation in asymmetric periodic loaded rib waveguides," *Appl. Phys. Lett.*, vol. 59, pp. 1278-1280, 1991.

[33] W. P. Huang and Z. M. Mao, "Polarization rotation in periodic loaded rib waveguides," *J. Lightwave Technol.*, vol. 10, pp. 1825-1831, Dec. 1992.

[34] J. J. G. M. van der Tol, F. Hakimzadeh, J. W. Pedersen, D. Li, and H. van Brug, "A new short and low-loss passive polarization converter on InP," *IEEE Photon. Technol. Lett.*, vol. 7, pp. 32-34, Jan. 1995

[35] T. Ando, T. Murata, H. Nakayama, J. Yamauchi, and H. Nakano, "Analysis and measurement of polarization conversion in a periodically loaded dielectric waveguide," *IEEE Photon. Technol. Lett.*, vol. 14, pp. 1288-1290, Sept. 2002.